Article

Cell Reports

Pharmacologic or Genetic Targeting of Glutamine Synthetase Skews Macrophages toward an M1-like Phenotype and Inhibits Tumor Metastasis

Graphical Abstract

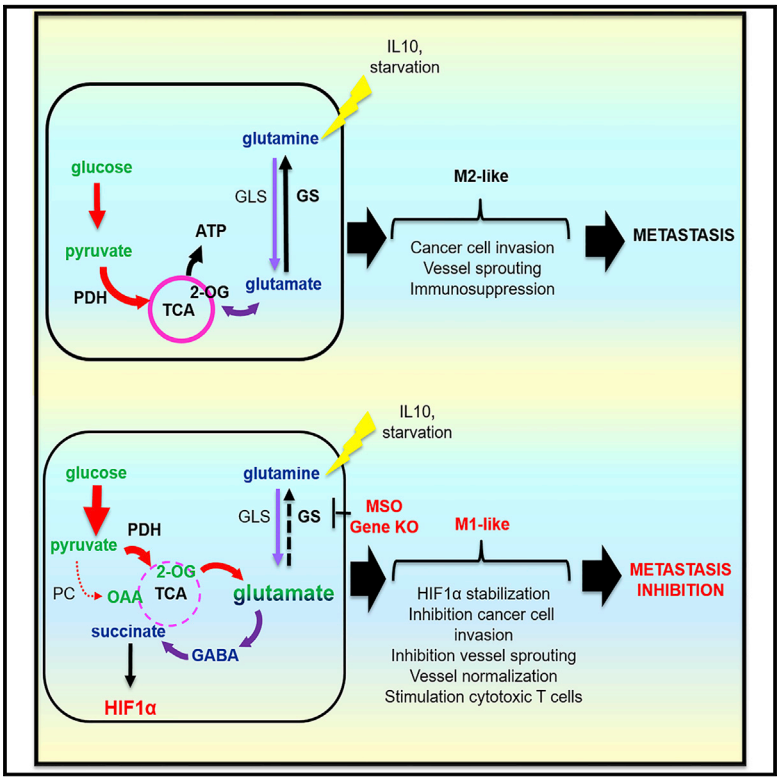

Highlights

- GS expression and activity are induced by M2 stimuli, especially under starvation
- Inhibition of GS activity skews M2 macrophages toward an M1-like phenotype
- Metabolic rewiring by GS loss favors immunostimulatory and antiangiogenic features
- GS ablation in macrophages blocks vessels, immunosuppression, and metastasis

Authors

Erika M. Palmieri, Alessio Menga, Rosa Martín-Pérez, ..., Attilio Guarini, Massimiliano Mazzone, Alessandra Castegna

Correspondence

massimiliano.mazzone@vib-kuleuven.be (M.M.),
alessandra.castegna@uniba.it (A.C.)

In Brief

Palmieri et al. show that inhibiting glutamine synthetase activity in M2 macrophages skews their polarization toward an HIF1α-mediated M1 state, which impairs cytotoxic T cell recruitment and angiogenesis. As a consequence of a more pronounced immunostimulatory and antiangiogenic effect, GS ablation in macrophages translates into prevention of metastasis.

Palmieri et al., 2017, Cell Reports *20*, 1654–1666
August 15, 2017
http://dx.doi.org/10.1016/j.celrep.2017.07.054

CellPress

OPEN ACCESS
CellPress

Cell Reports
Article

Pharmacologic or Genetic Targeting of Glutamine Synthetase Skews Macrophages toward an M1-like Phenotype and Inhibits Tumor Metastasis

Erika M. Palmieri,[1,2,12] Alessio Menga,[3,4,5,12] Rosa Martín-Pérez,[4,5,12] Annamaria Quinto,[3] Carla Riera-Domingo,[4,5] Giacoma De Tullio,[3] Douglas C. Hooper,[6] Wouter H. Lamers,[7,8,9] Bart Ghesquière,[10,11] Daniel W. McVicar,[2] Attilio Guarini,[3] Massimiliano Mazzone,[4,5,13,14,*] and Alessandra Castegna[1,3,14,*]

[1]Department of Biosciences, Biotechnologies and Biopharmaceutics, University of Bari, 70125 Bari, Italy
[2]The Cancer and Inflammation Program, National Cancer Institute-Frederick, Frederick, MD 21702, USA
[3]Hematology Unit, National Cancer Research Center, Istituto Tumori "Giovanni Paolo II," 70124 Bari, Italy
[4]Laboratory of Tumor Inflammation and Angiogenesis, Center for Cancer Biology (CCB), VIB, 3000 Leuven, Belgium
[5]Laboratory of Tumor Inflammation and Angiogenesis, Department of Oncology, KU Leuven, 3000 Leuven, Belgium
[6]Department of Cancer Biology, Department of Neurological Surgery, Thomas Jefferson University, Philadelphia, PA 19107, USA
[7]Department of Anatomy & Embryology, NUTRIM School for Nutrition and Translational Research in Metabolism, Maastricht University, 6211 LK Maastricht, the Netherlands
[8]Nutrigenomics Consortium, Top Institute Food and Nutrition, Wageningen, the Netherlands
[9]Tytgat Institute for Liver and Intestinal Research, Academic Medical Center, University of Amsterdam, 1012 WX Amsterdam, the Netherlands
[10]Metabolomics Expertise Center, Vesalius Research Center, VIB, 3000 Leuven, Belgium
[11]Metabolomics Expertise Center, Department of Oncology, KU Leuven, 3000 Leuven, Belgium
[12]These authors contributed equally
[13]Lead Contact
[14]Senior author
*Correspondence: massimiliano.mazzone@vib-kuleuven.be (M.M.), alessandra.castegna@uniba.it (A.C.)
http://dx.doi.org/10.1016/j.celrep.2017.07.054

SUMMARY

Glutamine-synthetase (GS), the glutamine-synthesizing enzyme from glutamate, controls important events, including the release of inflammatory mediators, mammalian target of rapamycin (mTOR) activation, and autophagy. However, its role in macrophages remains elusive. We report that pharmacologic inhibition of GS skews M2-polarized macrophages toward the M1-like phenotype, characterized by reduced intracellular glutamine and increased succinate with enhanced glucose flux through glycolysis, which could be partly related to HIF1α activation. As a result of these metabolic changes and HIF1α accumulation, GS-inhibited macrophages display an increased capacity to induce T cell recruitment, reduced T cell suppressive potential, and an impaired ability to foster endothelial cell branching or cancer cell motility. Genetic deletion of macrophagic GS in tumor-bearing mice promotes tumor vessel pruning, vascular normalization, accumulation of cytotoxic T cells, and metastasis inhibition. These data identify GS activity as mediator of the proangiogenic, immunosuppressive, and pro-metastatic function of M2-like macrophages and highlight the possibility of targeting this enzyme in the treatment of cancer metastasis.

INTRODUCTION

Macrophages are able to display different activation states in response to specific stimuli. Quiescent macrophages (M0) can be activated by interferon-γ (IFNγ) and Toll-like receptor (TLR) agonists toward an inflammatory (M1-like) phenotype, thus developing pro-inflammatory microbicidal and tumoricidal properties. However, under interleukin-4 (IL-4), IL-13, and IL-10 (M2-like activation), macrophages suppress inflammatory and adaptive Th1 responses by producing anti-inflammatory factors (IL-10, transforming growth factor β [TGF-β], and IL-1 receptor antagonist [IL-1Rα]), scavenging debris and promoting angiogenesis, tissue remodeling, and repair (Locati et al., 2013; Martinez et al., 2006). Lately, it has become evident that this phenotypic response to their microenvironment is transcriptionally and metabolically regulated (McGettrick and O'Neill, 2013; O'Neill and Hardie, 2013). Specific metabolic features have been associated with M1-like macrophages displaying enhanced glycolysis and reduced oxidative phosphorylation in contrast with more oxidative M2-like macrophages (Biswas and Mantovani, 2010). However, the functional valorization of these different metabolic reactions is far from being completed. Elucidation of these critical pathways might be significant in tumor-associated macrophages (TAMs), which can acquire pro-metastatic and angiogenic properties at the tumor site. Recent studies point to the role of environmental factors in primary tumors and how the targeting of these signals can suppress the immunosuppressive, pro-angiogenic, and pro-metastatic functions of TAMs (Casazza et al., 2013; Colegio et al., 2014; Wenes et al., 2016).

Glutamine synthetase (GS) is a key enzyme involved in nitrogen metabolism, acid-base homeostasis, and cell signaling across multiple species of prokaryotes and eukaryotes (Eisenberg et al., 2000). One of the main roles of GS in vertebrates is to produce glutamine from glutamate and ammonia, which are toxic to the CNS (Butterworth, 2003; Liu et al., 2013; Olney, 1990). Moreover, a continuous supply of glutamine is required for several physiological processes, including synthesis of glutamate and gamma-aminobutyric acid (GABA), synthesis of proteins, and osmoregulation (Norenberg et al., 2007). Expression of GS has been noted in different tumor cells, macrophages, and adipocytes (Chrétien et al., 2002; Hadden et al., 1997; Kocher et al., 2000; Kung et al., 2011). Interestingly the glutamine-producing activity of GS has recently been associated with important signaling mechanisms. GS activity inhibits the mammalian target of rapamycin (mTOR) pathway and induces autophagy in B cells (van der Vos et al., 2012). We have recently found that GS is expressed at later stages of adipocyte differentiation in a glucocorticoid-independent manner and desensitizes mature adipocytes to proinflammatory insults by raising intracellular glutamine levels, demonstrating a mechanism by which GS, through glutamine production, controls adipocyte response to pro-inflammatory stimuli (Palmieri et al., 2014). In murine microglia, GS activity controls the response to lipopolysaccharide (LPS) (Palmieri et al., 2017). GS is also capable of promoting T cells with high Foxp3 expression and regulatory properties in regulatory T cells (T_{regs}) (Metzler et al., 2016), whereas glutaminolysis induces an inflammatory anti-tumor (Th1) response in effector T cells and represses the formation of T_{reg} cells (Klysz et al., 2015). Finally, glutamine consumption is increased during classical macrophage activation (Curi et al., 2007; Murphy and Newsholme, 1998).

In the present study, we characterize the role of GS in modulating macrophage skewing toward the M2 phenotype. We show that GS expression primes primary human monocytes into M2 macrophages, whereas GS inhibition switches their phenotype toward a more M1-like phenotype through a specific metabolic rewiring involving succinate accumulation. The enhanced production of succinate is a critical regulator of the pro-inflammatory response, both through the inhibition of anti-inflammatory gene expression and via hypoxia inducible factor (HIF)-1α stabilization (Mills et al., 2016). Consistently, GS inhibition in macrophages translates into a strong functional impairment in terms of *in vitro* T cell recruitment and angiogenesis. Macrophage-specific knockout of GS results in a marked reduction in metastasis formation in mice. These findings establish GS as a main metabolic regulator of inflammation by modulating glutamine levels. Furthermore, selective targeting of GS in macrophages might effectively contrast metastatic processes, increasing the survival of malignant cancer patients.

RESULTS

GS Is Expressed in Alternatively Activated (M2-like) Macrophages

To evaluate the role of GS in the polarization of blood-derived human macrophages, we first tested GS protein expression in primary human resting macrophages (M0/resting), those with a proinflammatory phenotype (M1) induced by LPS/IFNγ, and with the alternatively activated phenotype (M2) elicited with IL-4 and IL-10, alone or in combination, or otherwise with a combination of the anti-inflammatory cytokines IL-4 and IL-13 with an overlapping function (Huang et al., 2015).

We found that GS protein was barely detected in M1 cells and more expressed in M2 cells (Figures 1A and 1B), particularly in IL-10-stimulated cells over all other anti-inflammatory stimuli, as detected through western blotting (Figure 1A). We then evaluated GS gene expression and activity levels during IL-10 stimulation of (M0) monocyte-derived macrophages (IL-10 macrophages in short). Two hours before stimulation with IL-10, cells were primed (or not) with the GS inhibitor methionine sulfoximine (MSO) at a concentration of 1 mM (MSO/IL-10 macrophages in short). Importantly, MSO is not toxic up to 5 mM (Figure S1). GS expression was increased in IL-10 and MSO/IL-10 compared with M0 cells (Figure 1C). Following GS expression, GS activity was also increased in IL-10-stimulated compared with M1 cells (Figure 1D). In line with this finding, intracellular glutamine levels were significantly higher in IL-10-derived M2 compared with M0 macrophages at 24 and 48 hr (Figure 1E). Treatment with the GS inhibitor MSO reduced intracellular glutamine levels at all times (Figure 1E). This indicates that the effect of GS inhibition is linked to the decrease in the intracellular levels of glutamine in IL-10 macrophages.

MSO Treatment of M2 Macrophages Promotes Succinate Accumulation and Glucose-Dependent Metabolism

Having established that GS is enriched in IL-10 macrophages, we aimed to characterize metabolism in IL-10-treated macrophages and the consequences of GS inhibition on these metabolic features (O'Neill and Pearce, 2016). Metabolites, together with ^{13}C incorporation levels from [U-^{13}C]-glutamine or [U-^{13}C]-glucose, were measured in LPS/IFNγ, IL-10, and MSO/IL-10 macrophages.

MSO treatment of IL-10 macrophages induces a significant rewiring of macrophage metabolism. As expected, MSO/IL-10 macrophages displayed much higher levels of glutamate compared with IL-10-treated macrophages. This was accompanied by a significant increase in the levels of succinate (Figure 2A), but not of other tricarboxylic acid (TCA) cycle intermediates (data not shown), and GABA, similar to LPS/IFNγ macrophages (Figure 2A). Interestingly, ^{13}C labeling experiments revealed that MSO treatment causes a significant shift from glutamine to glucose utilization for glutamate and TCA intermediate synthesis (Figures 2B–2F), as demonstrated by the consistent drop in ^{13}C labeling from glutamine and the increase in ^{13}C labeling from glucose in TCA cycle intermediates, with the exception of succinate (Figure 2G), in which there is a significant enrichment from ^{13}C glutamine. However, glutamine uptake is not reduced, as also suggested by upregulation of the glutamine transporter LAT1 in MSO/IL-10 compared with IL-10 macrophages (Figure 2H), but is sustained and rerouted to succinate synthesis, probably through the GABA shunt. Additionally, the slight ^{13}C enrichment in M+3 malate and citrate from glucose (Figure S2) clearly points to a small but significant

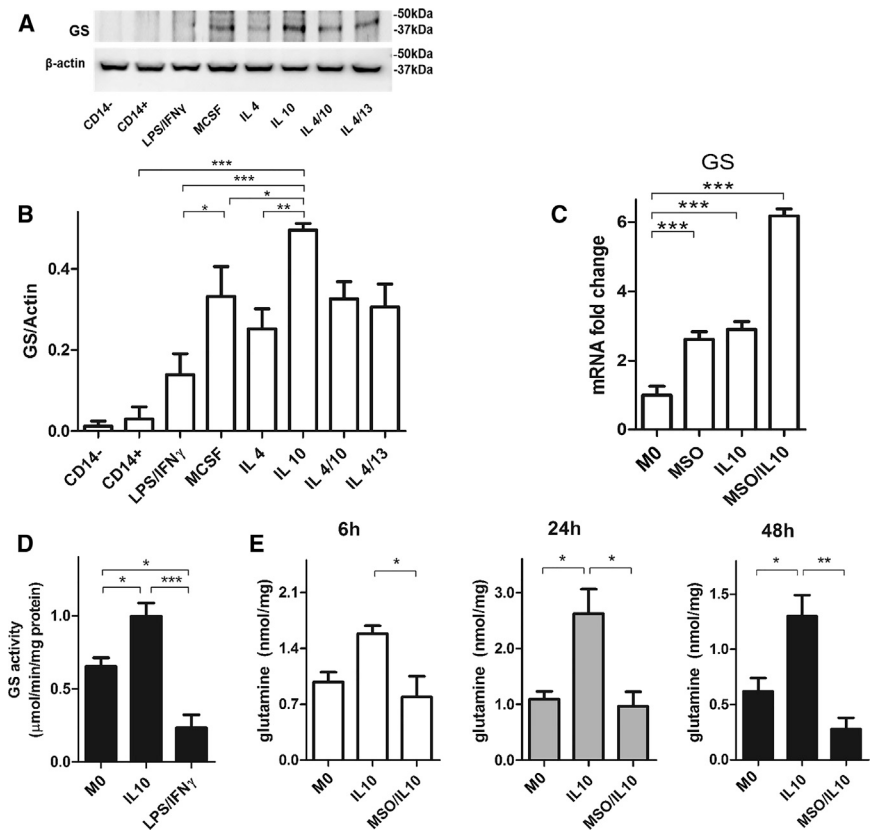

Figure 1. IL-10 Macrophages Display GS Expression and Activity

(A and B) GS and β-actin immunoblot (A) and densitometric levels (B) in human $CD14^-$, $CD14^+$ cells (monocytes), resting (M0, macrophage colony stimulating factor [MCSF]), and differently polarized monocytes-derived macrophages (LPS/IFNγ, IL-4, IL-10, IL-13, and a combination of those, with M-CSF) following 24 hr of activation (n = 3).

(C) GS expression levels in resting M0, IL-10, and MSO/IL-10 macrophages following 16 hr of activation with and without 2 hr of pre-incubation with MSO (n = 3).

(D) GS protein activity levels in resting (M0), LPS/IFNγ, and IL-10 macrophages following 24 hr of activation (n = 4).

(E) LC-MS/MS quantification of intracellular glutamine in resting (M0), IL-10, and MSO-treated IL-10 6, 24, and 48 hr after treatment (n = 4).

Data are means ± SEM. Western blots are representative of 3 independent experiments. *p < 0.05, **p < 0.001, ***p < 0.0001.

reprogramming of pyruvate metabolism toward oxaloacetate through pyruvic carboxylase (PC) (Fan et al., 2010; Le et al., 2012).

GS Inhibition Blocks M2-like Skewing and Promotes an M1-like Phenotype

Because succinate accumulation, increased glucose utilization, and PC activation are all features typical of classically activated macrophages, we investigated the functional consequences of GS inhibition on the differentiation state of primary human monocyte-derived macrophages primed in culture toward an anti-inflammatory phenotype. As expected, the M2 macrophage marker CD163 was strongly induced and pronouncedly expressed on the surface of macrophages by IL-10 (Figure 3A). GS inhibition strongly reduced IL-10-mediated upregulation of CD163 in macrophages (Figures 3A–3C). In IL-10-stimulated cells, expression of the costimulatory molecule CD80 was almost absent (Figure 3A) compared with expression of the same marker in endotoxin-stimulated cells (M1) (Figures 3A and 3B). Treatment with IL-10 in the presence of MSO induced the M1 phenotype in macrophages, as indicated by the strong appearance and upregulation of CD80 concomitant with disappearance of CD163 (Figure 3D).

Based on these results, we assessed the influence of GS on genes that are differentially expressed in M1 and M2 macrophages. GS inhibition in IL-10-stimulated macrophages upregulated the expression of genes preferentially found in M1 macrophages, such as TNF-α and NOS2 and, to a higher extent, CXCL9 and CXCL10 (Figure 3E; Figure S1B). MSO strongly prevented the induction of M2-specific markers upon IL-10 stimulation, such as MSR1 (CD204) and MRC1 (CD206), CCL17, and CCL18 (Figure 3E; Figure S1B). These data indicate that GS plays a positive role in M2 macrophage polarization and that GS blockade hinders the expression of M2 markers, whereas it promotes M1 markers.

To ascertain whether glutamate accumulation alone could be responsible for programming expression of specific markers of M1 macrophages, we treated IL-10 macrophages with the permeable dimethylglutamate (DMG). As shown in Figure 3F, incubation with 5 mM DMG in M2 macrophages is sufficient to induce a marked increase in M1 markers (Figure 3F) without influencing M2 markers (data not shown).

GS Inhibition Leads to HIF1α Activation

Having established that GS inhibition promotes an M1-like phenotype in macrophages in which the levels of succinate are increased, we then investigated the molecular mechanisms behind this functional reprogramming. Because succinate is known to stabilize HIF1α activity (Tannahill et al., 2013), we speculated that GS inhibition (and succinate accumulation) might promote a classical M1 phenotype through HIF1α activation (Takeda et al., 2010).

First of all, we assessed HIF1α transcriptional activity by expressing an inducible HIF-responsive firefly luciferase reporter in LPS/IFNγ, IL-10, and MSO/IL-10 macrophages. Luciferase activity was maximal in LPS/IFNγ, as expected, and very low in IL-10-treated macrophages (Figure 4A). MSO treatment completely reversed this activity in IL-10 macrophages because these cells exhibited luciferase signals comparable with

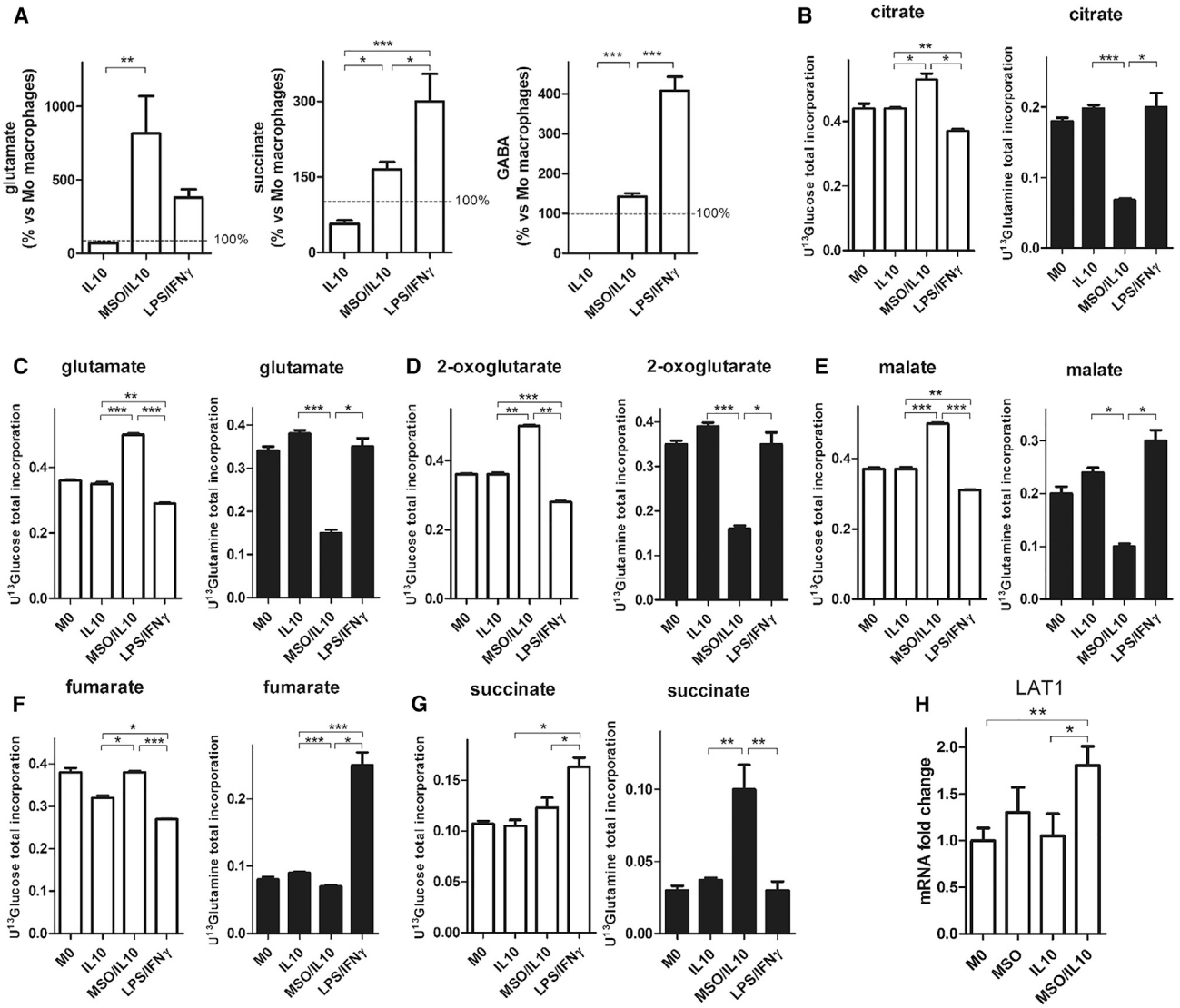

Figure 2. GS Inhibition Modifies Metabolite Levels in IL-10 versus LPS/IFNγ Macrophages

(A) Evaluation of glutamate, GABA, and succinate in IL-10, MSO/IL-10, and LPS/IFNγ versus resting (ctrl, 100%) macrophages (n = 6) following 24 hr of activation.

(B–G) Evaluation of the [U-^{13}C]-glutamine-derived (right) and [U-^{13}C]-glucose-derived (left) carbon incorporation levels into the TCA intermediates citrate (B), glutamate (C), 2 oxoglutarate (D), malate (E), fumarate (F), and succinate (G) in resting (M0), IL-10, and MSO-treated IL-10 versus LPS/IFNγ macrophages following 24 hr of activation (n = 4).

(H) LAT1 expression levels in resting M0, IL-10, and MSO/IL-10 macrophages following 16 hr of activation with and without previous MSO addition (n = 3).

Data are means ± SEM. *p < 0.05, **p < 0.001, ***p < 0.0001.

LPS/IFNγ macrophages. Inhibition of HIF1α activity in LPS/IFNγ and MSO/IL-10 cells through acriflavine treatment lowered the luciferase reporter signal to the levels of resting (M0) and IL-10 macrophages (Figure 4A). In line with this finding, the HIF1α protein levels in MSO/IL-10 and LPS/IFNγ were higher compared with IL-10 macrophages (Figure 4B).

Additionally, HIF1α inhibition by acriflavine treatment in MSO/IL-10 macrophages rescued the M2- to M1-like phenotype switching, as demonstrated by the decreased expression of markers typically expressed in classically activated macrophages, such as TNF-α, CXCL10, and inducible nitric oxide synthase (NOS2) (Figure 4C), and the concomitant increase of markers expressed in IL-10 macrophages, such as CCL17, MRS1, CCL18, and MRC1 (Figure 4C). Overall, these data support the idea that GS inhibition blocks the M2 skew by IL-10 and promotes an M1 phenotype, at least in part, via HIF1α, which can be possibly stabilized by succinate accumulation (Mills et al., 2016).

Starvation of M2 Macrophages Increases GS Expression

Since GS is known to respond to conditions of nutrient deprivation (van der Vos et al., 2012), we wanted to ascertain whether

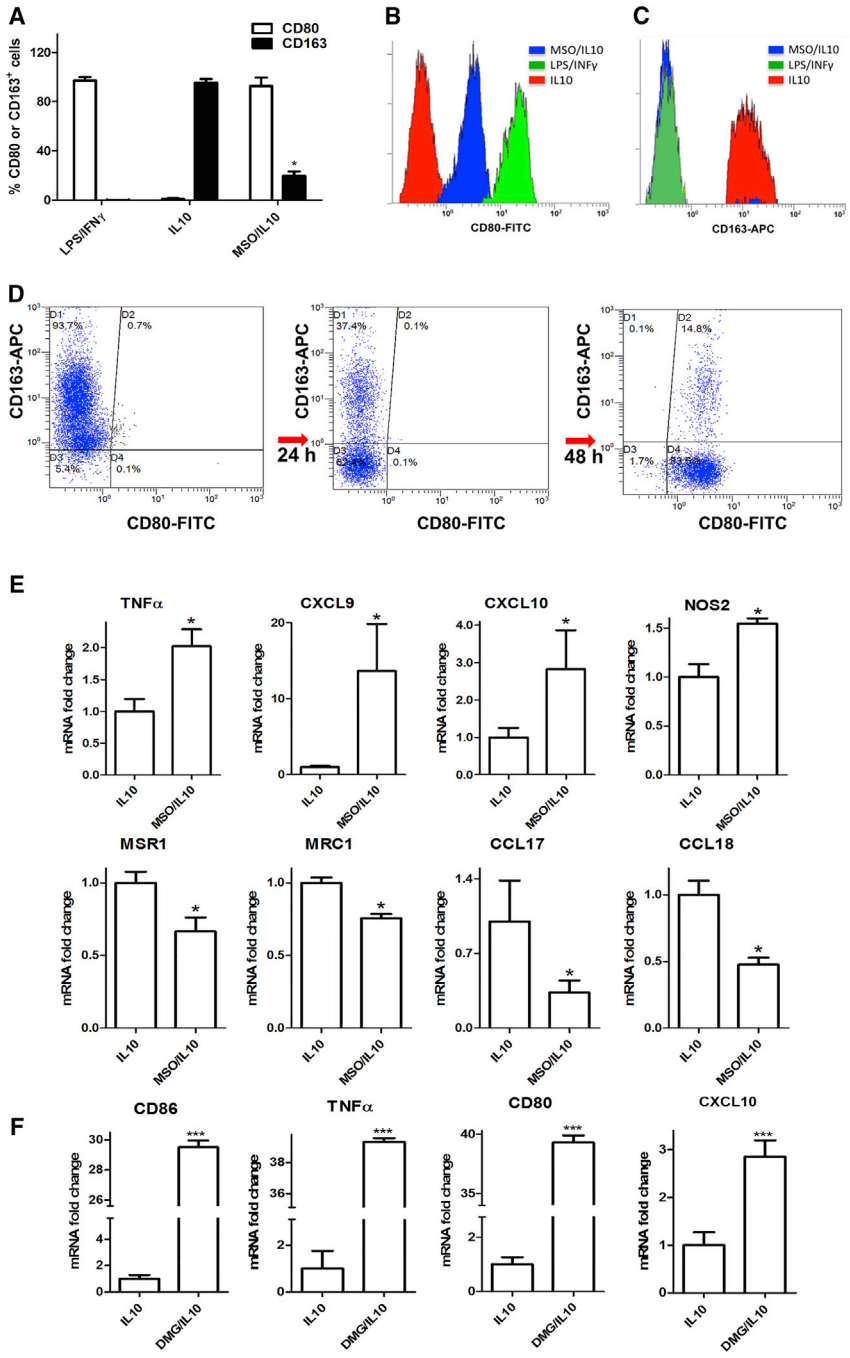

Figure 3. GS Inhibition Modifies Polarization of IL-10 Macrophages

(A) Flow cytometric quantification of the percentage of CD80$^+$ and CD163$^+$ cells after IL-10 treatment in the absence or presence of MSO versus LPS/IFNγ treatment following 24 hr of activation (n = 4).

(B and C) FACS quantification of CD80 (B) and CD163 (C) levels in IL-10 and MSO-treated IL-10 versus LPS/IFNγ macrophages as above.

(D) FACS dot plots depicting CD80 and CD163 modulation following MSO treatment in IL-10 macrophages.

(E) qRT-PCR quantification of M1 or M2 markers in macrophages. Top: fold increase of TNF-α, CXCL9, CXCL10, and NOS2 mRNA in IL-10 and MSO-treated IL-10 (n = 3). Bottom: fold reduction of MSR1, MRC1, CCL17, and CCL18 mRNA in IL-10 and MSO-treated IL-10 macrophages following 24 hr of activation with and without previous MSO addition (n = 3).

(F) qRT-PCR quantification of M1 markers in macrophages with DMG. Shown is the fold increase of CD86, TNF-α, CD80, and CXCL10 mRNA in IL-10 macrophages with and without 2 hr of pre-incubation with 5 mM DMG.

Data are means ± SEM. *p < 0.05. ***p < 0.0001.

this was the case in macrophages. As starvation enhanced GS expression in both M0 and IL-10 macrophages (Figure 5A), we hypothesized that starvation could promote M2 polarization by promoting GS expression irrespective of IL-10 treatment. With this aim, we cultured M0 macrophages in regular rich medium (2 mM glutamine and 11 mM glucose) or in deprived medium (2 mM glucose and 0.3 mM glutamine) without any additional stimulus and measured M2 and M1 markers. Expression of M2 markers was enhanced in starved compared with normally grown M0 macrophages (Figure 5B) without any change in M1 markers (data not shown). To shed light on the role of GS expression under starved conditions, we measured the levels of extracellular glutamine in starved M0 compared with LPS/IFNγ macrophages. In rich medium, glutamate uptake in M0 macrophages parallels that displayed by LPS/IFNγ, whereas extracellular glutamine levels displays differences in M0 compared with LPS/IFNγ macrophages, which reached statistical significance at 72 hr (Figure 5C). Under starved conditions, extracellular levels of glutamate markedly decreased under both conditions, whereas, under starvation, glutamine levels significantly increased at 48 hr and even more at 72 hr in M0 compared with LPS/IFNγ macrophages, in which glutamine levels did not change (Figure 5C). This suggests that glutamine produced by the activity of GS in M0 macrophages might be secreted into spent medium, and this is also corroborated by the increased expression levels of the cellular glutamine transporters ASCT2 and LAT1 (Figure 5D).

GS-Inhibited Macrophages Induce Lymphocyte Recruitment and Inhibit T Cell Suppression, Endothelial Cell (EC) Capillary Formation, and Cancer Cell Motility

Macrophages in their altered form are one of the major players to cause systemic fault of effector T cell functions (Kreider et al.,

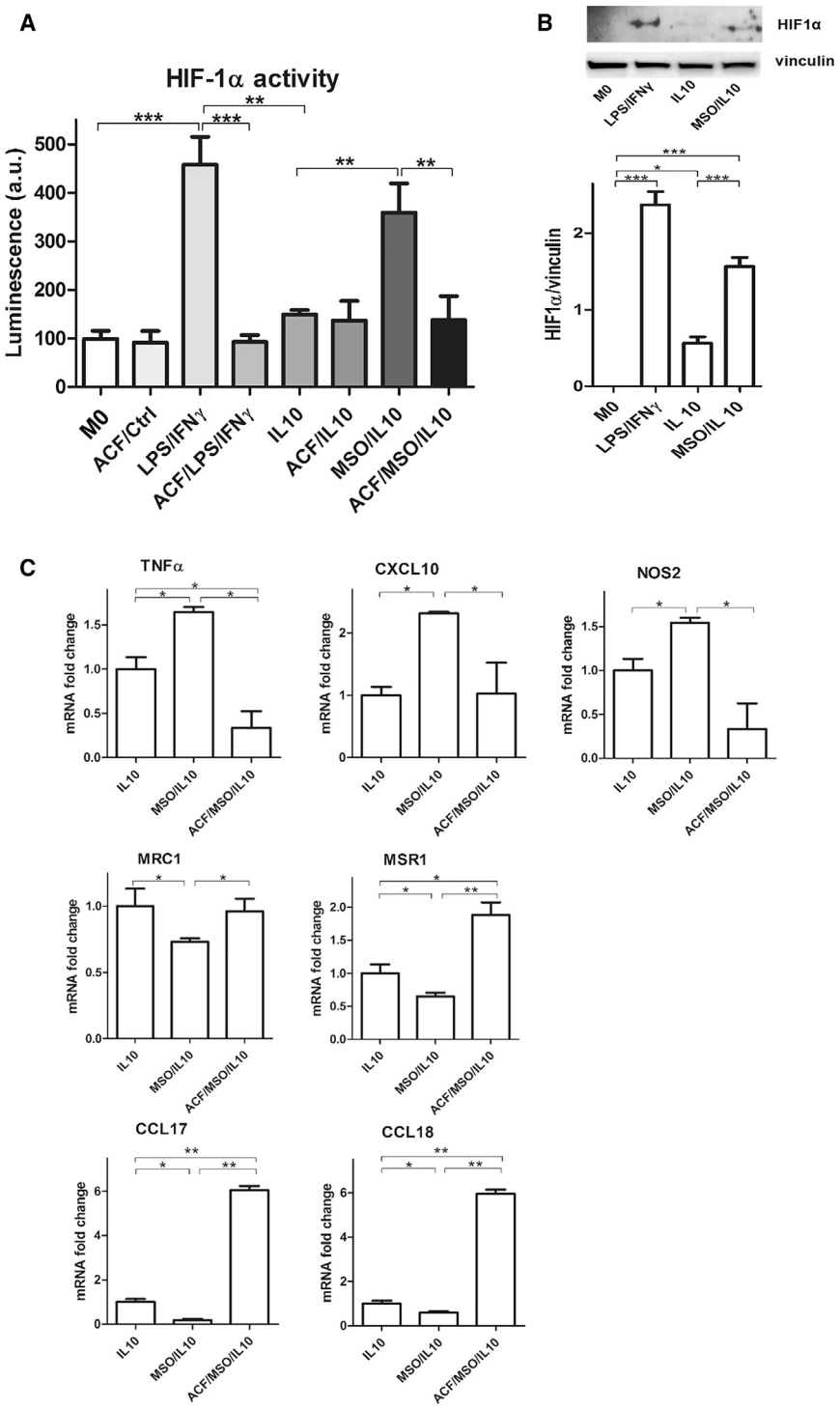

Figure 4. GS Inhibition Stabilizes HIF1α Activity

(A) Evaluation of HIF1α transcriptional activity in resting (M0) and IL-10 versus LPS/IFNγ macrophages after 16 hr of stimulation with and/or without previous MSO and acriflavine (ACF) addition (n = 3).

(B) Western blotting and densitometric analysis of HIF1α protein in M0, IL-10, and MSO-treated IL-10 versus LPS/IFNγ macrophages after 16 hr of stimulation (n = 3).

(C) qRT-PCR quantification of M1 or M2 markers in macrophages following HIF1α inhibition. Top: fold change of TNF-α, NOS2, and CXCL10 mRNA in IL-10 stimulated macrophages with and/or without previous MSO and ACF addition (n = 3). Bottom: fold change of MSR1, MRC1, CCL17, and CCL18 mRNA levels in macrophages as above (n = 3).

Data are means ± SEM. *p < 0.05, ***p < 0.0001.

2007). We then tested the relevance of GS inhibition in M2 macrophages for T cell suppression and migration. After MSO was washed out, resting M2 and M2/MSO macrophages were co-cultured with autologous $CD4^+$ and $CD8^+$ T cells. IL-10-derived M2 macrophages stimulated for 24 hr had the highest ability to suppress the proliferation of cocultured $CD4^+$ and $CD8^+$ T cells (–) (Figure 6E). Upon MSO treatment, IL-10 macrophages regained the ability to promote migration and recruitment of T cells (Figure 6E).

(Figures 6A and 6B). Priming with MSO blunted the T cell-suppressive phenotype of M2 macrophages because $CD4^+$ and $CD8^+$ T cell proliferation was partly rescued; however, this rescue was statistically significant with $CD8^+$ T cells only (Figures 6A and 6B). Nevertheless, the proliferation index (PI, the number of divisions divided by the number of cells that underwent division) significantly increased in both $CD4^+$ and $CD8^+$ cells when cultured with MSO/IL-10 versus IL-10 macrophages (Figure S3). We also evaluated the activation marker CD69 in T cell populations after coculture. We show that MSO/IL-10 macrophages induced a significant upregulation of CD69 expression on the surface of both $CD4^+$ and $CD8^+$ T cells compared with IL-10-stimulated macrophages and M0 resting cells (Figures 6C and 6D).

To evaluate the extent of adhesion and chemotaxis of T cells, $CD8^+$ lymphocytes were cultured either alone or with, respectively, LPS/IFNγ, IL-10, and MSO/IL-10 macrophages and stimulated with the chemoattractant CXCL10. The presence of the chemokine or of M1 macrophages elicited their chemotaxis through a 5-μm pore membrane, at variance with IL-10-treated macrophages and the condition without macrophages

Based on the previous findings, we next assessed the network of capillary formation promoted by M2 macrophages under conditions of GS inhibition. Compared with IL-10 macrophages,

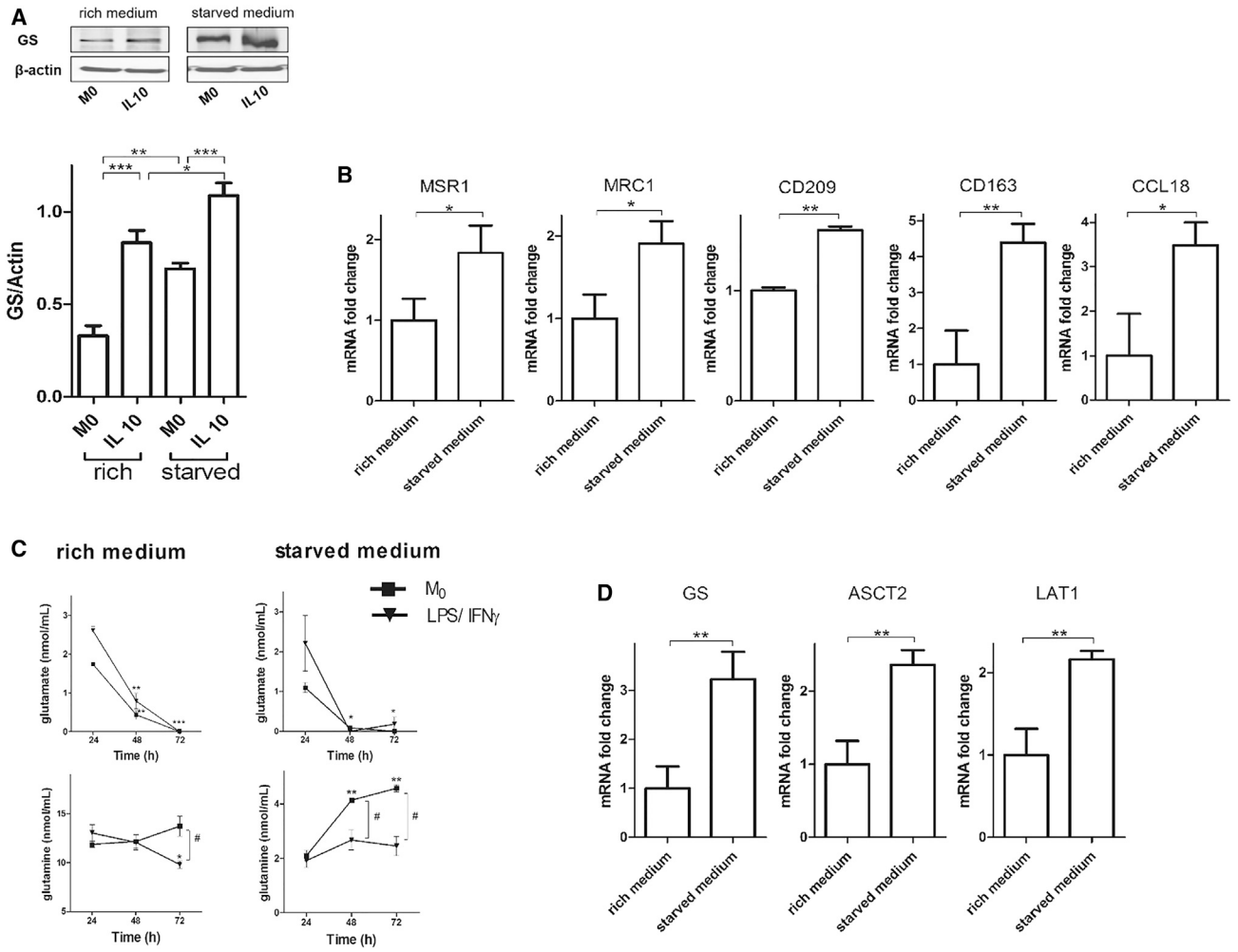

Figure 5. Starvation Enhances GS Expression in IL-10-Polarized Macrophages

(A) Western blotting and densitometric analysis of GS in resting (M0) and IL-10-treated macrophages in rich and starved medium after 60 hr of culture. Shown are representative lanes of the same western blot run and exposure. Data are means ± SEM. *$p < 0.05$, **$p < 0.001$ versus M0.

(B) qRT-PCR quantification of M2 markers under starved conditions. Shown are fold changes of MSR1, MRC1, CD209, CD163, and CCL18 mRNA in M0 macrophages in rich versus starved medium after 36 hr of culture (n = 3).

(C) Extracellular levels of glutamate and glutamine in rich and starved medium. Shown is quantification of glutamate and glutamine at 24, 48, and 72 hr of starvation (n = 3). Data are means ± SEM. *$p < 0.05$, **$p < 0.001$, ***$p < 0.0001$ in 72-hr- compared with 24-hr-starved cells. $^{\#}p < 0.05$ in M0 versus LPS/IFNγ-treated cells.

(D) qRT-PCR quantification of GS and the glutamine transporters under rich and starved conditions. Shown are fold changes of GS, ASCT2, and LAT1 mRNA in M0 macrophages in rich versus starved medium after 36 hr of culture (n = 3).

Where not indicated otherwise, data are means ± SEM. *$p < 0.05$, **$p < 0.001$.

MSO/IL-10 cells displayed a reduced ability to promote capillary formation, indicating that the MSO treatment is able to reduce the angiogenic phenotype of IL-10 macrophages (Figure 6F). Given the ability of M2 macrophages to sustain cancer cell motility (Joyce and Pollard, 2009), we set up a system where we assessed cancer migration trough 8-μm pores in the presence of IL-10 versus MSO/IL-10 macrophages. Consistent with the observation that GS inhibition prevents M2 features, cancer cell migration in the presence of MSO/IL-10 macrophages was 56% inhibited compared with the condition where IL-10-stimulated M2-like macrophages were present on the Transwell (Figure 6G). In line with a more M1-like phenotype, MSO/IL-10 macrophages behaved similarly to LPS/IFNγ macrophages (Figure 6G).

Hence, GS activity in IL-10-stimulated, M2-like macrophages is required to suppress $CD4^+$ and $CD8^+$ T cell proliferation and limit $CD8^+$ cell migration, whereas it promotes EC and cancer cell migration.

GS Deficiency in Tumor-Associated Macrophages Prevents Metastasis

To translate our findings *in vivo*, we specifically knocked out GS in macrophages upon administration of tamoxifen in

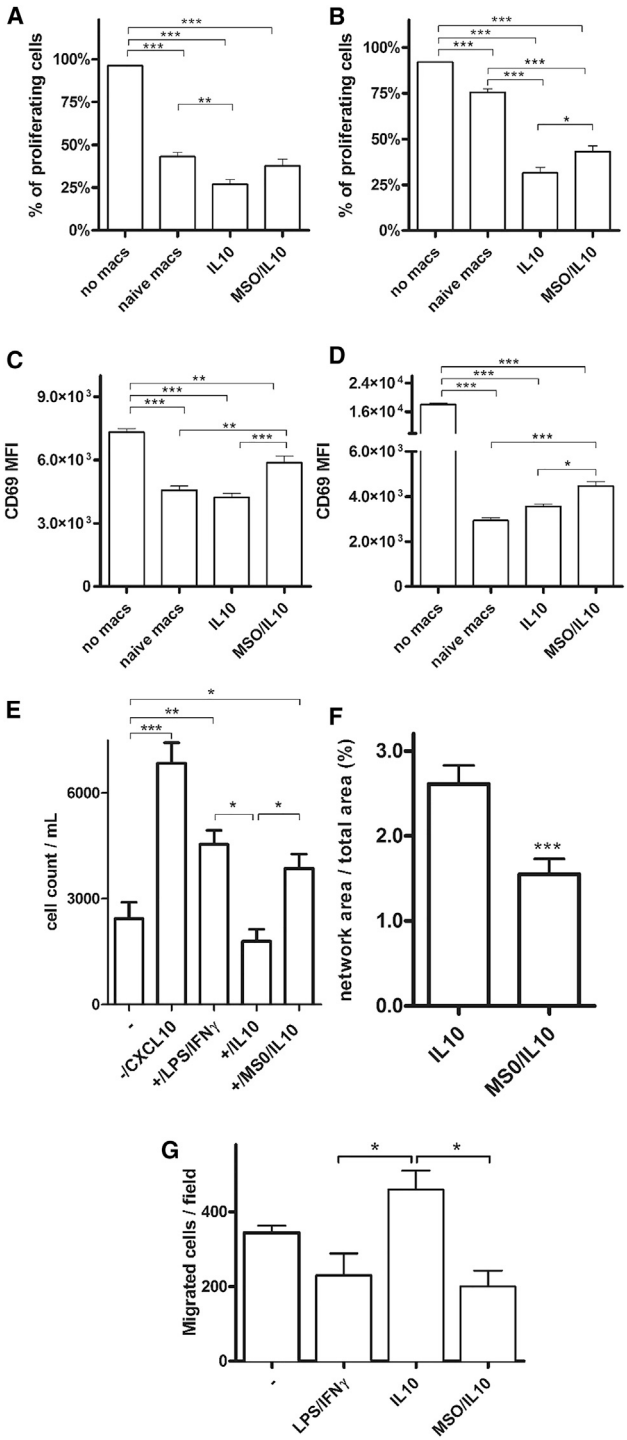

Figure 6. GS Targeting in Macrophages Prevents T Cell Suppression and Inhibits Endothelial Capillary Network Formation

(A and B) T cells labeled with cell trace violet (CTV) were stimulated with or without autologous macrophages in different ways. Five days later, the percentage of CTV-low cells, measured by flow cytometry, was used as a measure of $CD4^+$ (A) and $CD8^+$ (B) proliferation (n = 4).

(C and D) Evaluation of CD69 protein, expressed as mean fluorescence intensity (MFI), was determined by flow cytometry on the surface of responder $CD4^+$ (C) and $CD8^+$ T cells (D) after coculture with or without macrophages (n = 3).

(E) $CD8^+$ T cell recruitment by IL-10 and MSO-treated IL-10 macrophages versus LPS/IFNγ macrophages; the migration of T cells cultured without macrophages (–) in the presence of CXCL10 was used as a positive ctrl (n = 2).

(F) Quantification of the endothelial capillary network in the presence of macrophages pretreated for 24 hr with IL-10 or MSO/IL-10 after 4 hr of incubation with HUVEC cells (n = 8).

(G) Evaluation of cancer cell migration through a Matrigel-coated micropore filter in the absence (–) or presence of LPS/IFNγ, IL-10, and MSO/IL-10 prestimulated macrophages after 24 hr of incubation (n = 6).

Data are means ± SEM. *p < 0.05, **p < 0.001, ***p < 0.0001 versus IL-10.

GS-floxed mice expressing a tamoxifen-induced Cre under the macrophage promoter *Csf1r*, thus obtaining GS conditional knockout (cKO) mice (Experimental Procedures). After checking for macrophage-specific GS deletion (Figure 7A) and their metabolic features under stimulation (Figure S4), we implanted Lewis lung carcinoma (LLC) cells subcutaneously and monitored tumor growth. Although the tumor volumes and weights were always similar (Figures 7B and 7C), metastases in GS cKO versus GS wild-type (WT) mice were decreased 2-fold (Figure 7D). We then evaluated the features of the TAM infiltrate by fluorescence-activated cell sorting (FACS) and analyzed the expression of the M1-like marker major histocompatibility complex class II (MHC class II) and the M2-like marker CD206 (MRC1) on the cell membrane of $F4/80^+$ cells (Laoui et al., 2014). Despite the overall macrophage abundance, in the tumor being comparable in both genotypes (Figure 7E; Figures S5A and S5B), we confirmed that GS cKO TAMs were prevalently MHC class II^{high} and $CD206^{low}$ (M1-like) compared with the WT controls that displayed mostly an MHC class II^{low} and $CD206^{high}$ (M2-like) phenotype (Figures 7F and 7G). Furthermore, GS cKO TAMs displayed higher levels of intracellular glutamate and succinate but lower levels of glutamine, as shown by MSO/IL-10-treated macrophages (Figures 7H–7J). Finally, reduced expression of the M2-specific markers *Arg1*, *Mrc1*, *Ccl17*, and *Ccl22* further confirmed that GS KO TAMs were skewed away from the M2-like phenotype (Figures 7K–7N).

To validate our *in vitro* observation that GS inhibition leads to a less immunosuppressive phenotype, we quantified intratumoral T cells in GS cKO versus WT mice. Although $CD4^+$ T cells were comparable in both genotypes (Figure S5C), cytotoxic $CD8^+$ T cells were increased by 75% upon GS deletion in TAMs (Figure 7O).

We also studied the tumor vasculature, and, according to the shift in macrophage phenotype, we found a decrease in CD31 staining in tumors from GS cKO versus WT mice (Figures 7P and 7Q). However, tumor vessels in GS cKO mice displayed increased functionality and vascular integrity, as indicated, respectively, by reduced tumor hypoxia and decreased accumulation of leaked red blood cells in the perivascular space (Figures 7R–7U). To exclude any artifacts derived from the expression of Cre in KO TAMs only, we compared GS cKO mice with heterozygous controls (carrying the Cre transgene as well) and confirmed all of the key features described above (Figure S6). Altogether, these data demonstrate that the inhibition of GS in TAMs hinders their angiogenic, immunosuppressive, and pro-metastatic potential.

DISCUSSION

TAMs are known to actively participate in the metastatic process by contributing to different steps in the metastatic cascade (Pollard, 2004). Indeed, TAMs do not only allow the tumor to escape the immune system but also promote angiogenic and lymphangiogenic sprouting, allowing cancer cells to escape through the vascular and lymphatic system, and, importantly, contribute to the formation of discontinuous, poorly covered, and leaky blood vessels that, because of their poor functionality, will not be able to restore oxygenation (Casazza et al., 2013; Condeelis and Pollard, 2006; Rolny et al., 2011). The lack of oxygen (hypoxia) and transient vascular permeability ultimately favor metastasis (Casanovas et al., 2005; Kerbel, 2005; Mazzone et al., 2009). It follows that antibodies blocking CSF1R, the receptor for the most relevant macrophage growth factor, CSF1, reduces circulating cancer cells and metastasis (Ries et al., 2014; Wyckoff et al., 2004).

Recently, metabolism has been highlighted as an important mediator of macrophage function through the discovery of the mechanisms that, behind these metabolic changes, strongly affect immune function (Galván-Peña and O'Neill, 2014), potentially modulating cancer development and metastasis formation. Here we identify a metabolic mechanism in macrophages that promotes protumoral and metastatic activities. GS activity and increased glutamine production provide metabolic conditions leading to the accumulation of M2-like, pro-metastatic macrophages (Figure S7). Besides its channeling into the TCA cycle, glutamine contributes to nucleotide and uridine diphosphate *N*-acetylglucosamine (UDP-GlcNAc) synthesis for support of protein folding and trafficking (Wellen and Thompson, 2012). In M2 macrophages, the glutamine route toward UDP-GlcNAc is particularly enhanced (Jha et al., 2015) because the molecule represents a building block for the synthesis of glycosylation moieties of lectin/mannose receptors, which, in their highly glycosylated form, are among the most typical M2 polarization markers (Sica and Mantovani, 2012). GS may then be crucial to sustain the M2 phenotype.

The relevance of GS in IL-10-stimulated macrophages is evident from the profound metabolic changes following GS inhibition and the subsequent functional deviation. Indeed, MSO treatment in IL-10 macrophages produces a strong intracellular accumulation of glutamate, which is probably a result of the cell's inability to synthesize glutamine and remove ammonia. We show that abnormal glutamate alone is capable of skewing IL-10 macrophages toward a proinflammatory phenotype. However, MSO-inhibited macrophages display all the typical features of M1-like macrophages in which HIF1α is stabilized, such as enhanced glycolysis and increased M1 marker expression and typical functional behavior (Corcoran and O'Neill, 2016). Our results support a role of succinate as a pro-inflammatory metabolite that accumulates from glutamine through the GABA shunt. Because succinate is a critical regulator of the pro-inflammatory response, both through the inhibition of anti-inflammatory gene expression and via HIF1α stabilization (Mills et al., 2016); accumulation of this metabolite under conditions of GS inhibition might conceivably relate to the measured increased HIF1α activity. However, given the spectrum of metabolic changes described here, other HIF1-independent mechanisms can underline this phenotypic change in GS-inhibited macrophages.

The *in vitro* data are confirmed in an *in vivo* murine model of conditional GS deletion in TAMs in which metastasis formation is significantly reduced compared with control mice. Although restricted to a single tumor type, these results strongly support the idea that GS activity is important for the proangiogenic, immunosuppressive, and pro-metastatic function of M2-like macrophages. Accumulation of MHC class II^{high} CD206^{low} M1-like macrophages following genetic deletion of GS is associated with a reduced metastatic burden (Figure 7) without altering the size of the primary tumor. This phenomenon can be explained by the contribution of TAMs to promoting distant cancer cell dissemination more than their relevance to tumor growth (Qian et al., 2015). However, such an effect on metastasis can be also indirect and, because of tumor vascular normalization, linked to reduced hypoxia and vessel permeability, in line with our previous reports (Leite de Oliveira et al., 2012; Mazzone et al., 2009; Rolny et al., 2011). Obviously, increased immunosurveillance as suggested by augmented CD8^{+} cytotoxic T-lymphocyte (CTL) cells can also hinder metastatic outgrowth, as previously shown by others (Eyles et al., 2010). What is certain is that the inhibition of metastasis observed in our mouse model can be ascribed to several factors and functions derived by GS-deficient, M1-repolarized TAMs (Pollard, 2004; Rolny et al., 2011).

It is worth noting that GS expression significantly senses nutrient deprivation because its expression level is under the control of FOXO3A (van der Vos et al., 2012). We confirm that M2-polarized macrophages under conditions of glutamine starvation enhance GS expression compared with those grown in high-nutrient medium, as already described for other cellular models (van der Vos et al., 2012). M0 macrophages (which weakly express GS) significantly increase GS protein levels following starvation, and this event is sufficient to skew cells toward an M2-like phenotype without any further cytokine treatment, in line with the role of nutrient deprivation in modifying the phenotype of macrophages, as described previously (O'Neill and Hardie, 2013). More interestingly, starvation in M0 macrophages promotes glutamine secretion, which is sustained by the upregulation of the cellular glutamine transporters. This clearly suggests that GS expression (which is enhanced under starved conditions) not only induces an M2-like polarization of macrophages but may also promote glutamine secretion for use by other cells.

In conclusion, our data suggest a functional role of glutamate-to-glutamine conversion in M2 macrophages that is relevant for the promotion of their immunosuppressive and proangiogenic state, which is ultimately relevant for metastasis formation. The present work highlights the role of metabolism rewiring as a way to manipulate macrophage functions, suggesting the importance of metabolic immunotherapeutic strategies in the fight against cancer.

EXPERIMENTAL PROCEDURES

More detailed methods are described in the Supplemental Experimental Procedures.

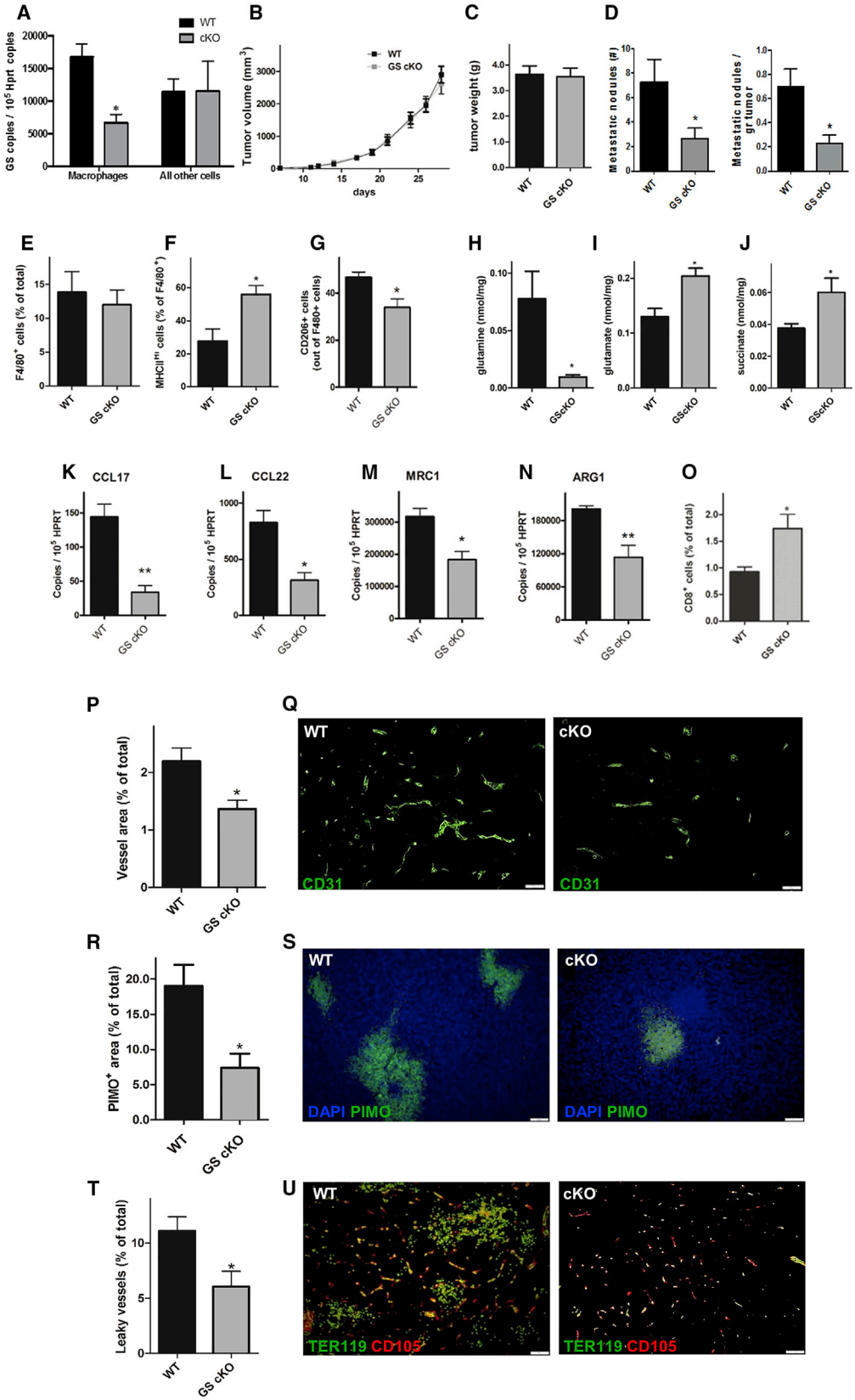

(legend on next page)

Animals

Experiments with control and GS cKO mice were obtained from about 8-week-old gender- and age-matched C57BL/6 littermates raised in a strictly controlled environment. Colony-stimulating factor receptor 1 (CSF1R)-CreERT transgenic mice (CSF1R-CreERT$^{Tg/WT}$), provided by J. Pollard (University of Edinburgh, UK), in which a tamoxifen-induced Cre is under the transcriptional control of the human *CSF1R* promoter, were crossed with GS-floxed mice (GS$^{L/L}$). The colony was bred by intercrossing GS$^{L/L}$;CSF1R-CreERT$^{Tg/WT}$ with GS$^{L/L}$;CSF1R-CreERT$^{WT/WT}$ mice or GS$^{L/L}$;CSF1R-CreERT$^{Tg/WT}$ with GS$^{L/WT}$;CSF1R-CreERT$^{Tg/WT}$ mice. All mice were treated with intraperitoneally (i.p.) injected tamoxifen (1 mg/mouse/day) for 5 days before subcutaneous implantation of LLC cancer cells. Tamoxifen-treated GS$^{L/L}$;CSF1R-CreERT$^{Tg/WT}$ mice were designated GS cKO mice, whereas GS$^{L/L}$;CSF1R-CreERT$^{WT/WT}$ mice or GS$^{L/WT}$;CSF1R-CreERT$^{Tg/WT}$ mice were used as control mice and denoted as WT or heterozygous (HET), respectively. Construction of targeting vectors and pup genotyping were performed as reported previously (He et al., 2010). 1 × 10^6 LLC adherent growing murine cells were injected subcutaneously. Volumes were measured three times a week using the formula $V = \pi \times d^2 \times D/6$, where d is the minor tumor axis and D is the major tumor axis. At the end stage, tumor weight was registered, and lung metastasis nodules were counted after intratracheal injection of 15% India ink solution (Finisguerra et al., 2015). Housing and all experimental animal procedures were approved by the Institutional Animal Care and Research Advisory Committee of the KU Leuven.

Cell Isolation and Culture

Human monocytes were obtained from healthy blood donor buffy coats under an institutional review board-approved protocol and isolated with CD14 MicroBeads (Miltenyi Biotec) as described previously (Palmieri et al., 2015). After differentiation, macrophages were stimulated with LPS/IFNγ (for M1 polarization), IL-4, IL-10, or a combination of both IL-4 and IL-10 (for M2 polarization). Experiments of inhibition were performed using 1 mM MSO, an irreversible inhibitor of GS, 1 hr before adding cytokines for activation. When starved, macrophages were transferred, for the last 36 hr of their differentiation, into RPMI medium containing 2 mM glucose and 0.3 mM glutamine. Cells were then stimulated with cytokines at the indicated times.

RNA and Protein Expression Analysis

RNA isolation and subsequent qRT-PCR analysis as well as protein extraction and western blot analysis were performed as described before (Menga et al., 2015; Palmieri et al., 2014; Prosniak et al., 2013). Glutamine quantification by liquid chromatography-tandem mass spectrometry (LC-MS/MS) was achieved as described previously (Palmieri et al., 2014), whereas GS enzymatic activity was measured as indicated (Castegna et al., 2011).

^{13}C Tracing Experiments

For metabolite analysis using mass spectrometry, cells were cultured for 24 hr in glucose- and glutamine-free DMEM with dialyzed fetal bovine serum (FBS), and the appropriate tracer was added. [U-^{13}C]-glutamine and [U-^{13}C]-glucose were from Sigma-Aldrich and Cambridge Isotopes Laboratories, respectively. Samples were extracted and analyzed as described in the Supplemental Experimental Procedures.

HIF1α-Responsive Luciferase Reported Expression

To express an inducible HIF-responsive firefly luciferase reporter, a pRRL-H3RO (Leite de Oliveira et al., 2012) plasmid vector was used. Human macrophages (4 × 10^4) were seeded in a 96-well plate in RPMI and 10% FBS as described before and transfected on day 7 of differentiation After 24 hr, cells were stimulated with LPS/IFNγ or IL-10 with and/or without 2 hr of pre-incubation with 1 mM MSO and 5 μM acriflavine (ACF). After 16 hr, the same amount of protein extract was read in a luminometer (Takeda et al., 2011).

CD4$^+$ and CD8$^+$ T Cell Purification and Expansion and CD8$^+$ Transmigration Assay

CD4$^+$ and CD8$^+$ cells were purified by magnetic assisted cell sorting (MACS) as described elsewhere (Barik et al., 2013), activated, expanded, and co-cultured with M2 and M2 plus MSO. Proliferation was measured, and suppression was calculated as in the Supplemental Experimental Procedures.

Migration of CD8$^+$ cells in response to macrophage-secreted factors was assessed by using Transwell permeable supports with a 5-μm porous polycarbonate membrane (Costar). LPS/IFNγ and IL-10 stimulated macrophages with or without MSO and CD8$^+$ cells were incubated for 3 hr at 37°C, and migrated cells were collected and counted under a microscope (Finisguerra et al., 2015) as described in the Supplemental Experimental Procedures.

EC Capillary Formation

2 × 10^5 human differentiated macrophages were embedded in Matrigel (BD Biosciences). After 4 hr of preconditioning, 1 × 10^4 human umbilical vein endothelial cell (HUVEC) fluorescently labeled with PKH-26 (Sigma-Aldrich) were added to the Matrigel. After 4 hr, HUVEC capillary formation was analyzed by measuring the number and length of branches using ImageJ software.

Statistical Analysis

Data entry and all analyses were performed in a blinded fashion. Results are shown as means ± SEM. Statistical significance was calculated by two-tailed unpaired t test or ANOVA test with Tukey post hoc test and considered statistically significant as follows: *p < 0.05, **p < 0.001, ***p < 0.0001.

Figure 7. Genetic Deletion of GS in TAMs Induces an M1-like Phenotype and CTL Accumulation, Inhibits Metastasis, and Induces Vessel Normalization

(A) Efficiency and specificity of genetic deletion in cKO mice measured by qRT-PCR on GS mRNA in F4/80$^+$ macrophages and F4/80$^-$ splenocytes, freshly sorted after 5-day *in vivo* treatment with tamoxifen (n = 3).

(B and C) Subcutaneous LLC tumor growth over time (B) and end-stage tumor weight (C) in wild-type (WT) and macrophage-specific knockout (cKO) mice (pool of 3 independent experiments, total n = 25).

(D) Number of lung metastases and lung metastatic index (the number of lung metastatic nodules divided by the corresponding tumor weight) in WT and macrophage-specific knockout (cKO) mice (pool of 3 independent experiments, total n = 25).

(E–G) FACS quantification of total F4/80$^+$ TAMs (E), M1-like MHC class II^{high} TAMs (F), and CD206-positive TAMs (G) in WT and macrophage-specific knockout (cKO) mice (n = 4).

(H–J) Evaluation of glutamine (H), glutamate (I), and succinate (J) in WT and macrophage-specific knockout (cKO) mice (n = 4).

(K–N) qRT-PCR quantification of CCL17 (K), CCL22 (L), MRC1 (M), AND ARG1 (N) in WT and macrophage-specific knockout (cKO) mice (n = 4).

(O) FACS quantification of CD8$^+$ cytotoxic T cells in WT and macrophage-specific knockout (cKO) mice (n = 4).

(P and Q) Quantification (P) and representative images (Q) of the CD31$^+$ tumor vessel area in WT and macrophage-specific knockout (cKO) mice (n = 8). The vessel area was calculated by the percentage of CD31 area per field.

(R and S) Quantification (R) and representative images (S) of pimonidazole (PIMO)$^+$ tumor hypoxic areas in WT and macrophage-specific knockout (cKO) mice (n = 8).

(T and U) Quantification (T) and representative images (U) of leaky vessels in WT and macrophage-specific knockout (cKO) mice, measured as the percentage of endoglin/CD105$^+$ vessels surrounded by lakes of TER119$^+$ red blood cells over the total number of vessels (n = 8). In each immunofluorescence quantification, n represents the number of animals. Six images per tumor were analyzed.

Scale bars, 100 μm. All graphs show mean ± SEM. *p < 0.05 versus the WT. See also Figures S1 and S2.

SUPPLEMENTAL INFORMATION

Supplemental Information includes Supplemental Experimental Procedures and seven figures and can be found with this article online at http://dx.doi.org/10.1016/j.celrep.2017.07.054.

AUTHOR CONTRIBUTIONS

A.C. and M.M. designed the research. E.M.P., R.M.P., A.M., G.D.T., A.Q., C.R.D., and B.G. performed the research. D.C.H., A.G., W.H.L., and D.W.M. provided expertises and contributed reagents. E.M.P., R.M., A.M., and G.D.T. analyzed the data. A.C. and M.M. wrote the manuscript.

ACKNOWLEDGMENTS

The authors are very grateful to J. Pollard for providing the CSF1R-CreERT$^{Tg/WT}$ mouse. B.G. was hosted by the University of Bari as a visiting scientist. A.C. is supported by grants from the University of Bari. M.M. is supported by an ERC starting grant (OxyMO, 308459) and by the following Belgian funding: FWO (G066515N) and STK (2014-197). R.M.P. and C.R.D. are supported by FWO postdoctoral and Ph.D. fellowships (12N4915N and 1108917N, respectively). E.M.P. and A.M. were both short-term EMBO fellows at the University of Leuven. The authors would also like to thank J. Subleski (from The Cancer and Inflammation Program, National Cancer Institute-Frederick, Frederick, MD 21702, USA) for technical assistance. The content of this paper does not necessarily reflect the views or policies of the Department of Health and Human Services USA, nor does mention of trade names, commercial products, or organizations imply endorsement by the US government. This work was funded, in part, by the Intramural Program of the National Institutes of Health, National Cancer Institute.

Received: May 10, 2016
Revised: May 30, 2017
Accepted: July 19, 2017
Published: August 15, 2017

REFERENCES

Barik, S., Banerjee, S., Mallick, A., Goswami, K.K., Roy, S., Bose, A., and Baral, R. (2013). Normalization of tumor microenvironment by neem leaf glycoprotein potentiates effector T cell functions and therapeutically intervenes in the growth of mouse sarcoma. PLoS ONE *8*, e66501.

Biswas, S.K., and Mantovani, A. (2010). Macrophage plasticity and interaction with lymphocyte subsets: cancer as a paradigm. Nat. Immunol. *11*, 889–896.

Butterworth, R.F. (2003). Hepatic encephalopathy. Alcohol Res. Health *27*, 240–246.

Casanovas, O., Hicklin, D.J., Bergers, G., and Hanahan, D. (2005). Drug resistance by evasion of antiangiogenic targeting of VEGF signaling in late-stage pancreatic islet tumors. Cancer Cell *8*, 299–309.

Casazza, A., Laoui, D., Wenes, M., Rizzolio, S., Bassani, N., Mambretti, M., Deschoemaeker, S., Van Ginderachter, J.A., Tamagnone, L., and Mazzone, M. (2013). Impeding macrophage entry into hypoxic tumor areas by Sema3A/Nrp1 signaling blockade inhibits angiogenesis and restores antitumor immunity. Cancer Cell *24*, 695–709.

Castegna, A., Palmieri, L., Spera, I., Porcelli, V., Palmieri, F., Fabis-Pedrini, M.J., Kean, R.B., Barkhouse, D.A., Curtis, M.T., and Hooper, D.C. (2011). Oxidative stress and reduced glutamine synthetase activity in the absence of inflammation in the cortex of mice with experimental allergic encephalomyelitis. Neuroscience *185*, 97–105.

Chrétien, F., Vallat-Decouvelaere, A.V., Bossuet, C., Rimaniol, A.C., Le Grand, R., Le Pavec, G., Créminon, C., Dormont, D., Gray, F., and Gras, G. (2002). Expression of excitatory amino acid transporter-2 (EAAT-2) and glutamine synthetase (GS) in brain macrophages and microglia of SIVmac251-infected macaques. Neuropathol. Appl. Neurobiol. *28*, 410–417.

Colegio, O.R., Chu, N.-Q., Szabo, A.L., Chu, T., Rhebergen, A.M., Jairam, V., Cyrus, N., Brokowski, C.E., Eisenbarth, S.C., Phillips, G.M., et al. (2014). Functional polarization of tumour-associated macrophages by tumour-derived lactic acid. Nature *513*, 559–563.

Condeelis, J., and Pollard, J.W. (2006). Macrophages: obligate partners for tumor cell migration, invasion, and metastasis. Cell *124*, 263–266.

Corcoran, S.E., and O'Neill, L.A.J. (2016). HIF1α and metabolic reprogramming in inflammation. J. Clin. Invest. *126*, 3699–3707.

Curi, R., Newsholme, P., Procopio, J., Lagranha, C., Gorjão, R., and Pithon-Curi, T.C. (2007). Glutamine, gene expression, and cell function. Front. Biosci. *12*, 344–357.

Eisenberg, D., Gill, H.S., Pfluegl, G.M., and Rotstein, S.H. (2000). Structure-function relationships of glutamine synthetases. Biochim. Biophys. Acta *1477*, 122–145.

Eyles, J., Puaux, A.-L., Wang, X., Toh, B., Prakash, C., Hong, M., Tan, T.G., Zheng, L., Ong, L.C., Jin, Y., et al. (2010). Tumor cells disseminate early, but immunosurveillance limits metastatic outgrowth, in a mouse model of melanoma. J. Clin. Invest. *120*, 2030–2039.

Fan, T.W., Yuan, P., Lane, A.N., Higashi, R.M., Wang, Y., Hamidi, A.B., Zhou, R., Guitart, X., Chen, G., Manji, H.K., and Kaddurah-Daouk, R. (2010). Stable isotope-resolved metabolomic analysis of lithium effects on glial-neuronal metabolism and interactions. Metabolomics *6*, 165–179.

Finisguerra, V., Di Conza, G., Di Matteo, M., Serneels, J., Costa, S., Thompson, A.A.R., Wauters, E., Walmsley, S., Prenen, H., Granot, Z., et al. (2015). MET is required for the recruitment of anti-tumoural neutrophils. Nature *522*, 349–353.

Galván-Peña, S., and O'Neill, L.A.J. (2014). Metabolic reprograming in macrophage polarization. Front. Immunol. *5*, 420.

Hadden, T.J., Ryou, C., and Miller, R.E. (1997). Elements in the distal 5′-flanking sequence and the first intron function cooperatively to regulate glutamine synthetase transcription during adipocyte differentiation. Nucleic Acids Res. *25*, 3930–3936.

He, Y., Hakvoort, T.B.M., Vermeulen, J.L.M., Labruyère, W.T., De Waart, D.R., Van Der Hel, W.S., Ruijter, J.M., Uylings, H.B.M., and Lamers, W.H. (2010). Glutamine synthetase deficiency in murine astrocytes results in neonatal death. Glia *58*, 741–754.

Huang, X.-L., Wang, Y.-J., Yan, J.-W., Wan, Y.-N., Chen, B., Li, B.-Z., Yang, G.-J., and Wang, J. (2015). Role of anti-inflammatory cytokines IL-4 and IL-13 in systemic sclerosis. Inflamm. Res. *64*, 151–159.

Jha, A.K., Huang, S.C.-C., Sergushichev, A., Lampropoulou, V., Ivanova, Y., Loginicheva, E., Chmielewski, K., Stewart, K.M., Ashall, J., Everts, B., et al. (2015). Network integration of parallel metabolic and transcriptional data reveals metabolic modules that regulate macrophage polarization. Immunity *42*, 419–430.

Joyce, J.A., and Pollard, J.W. (2009). Microenvironmental regulation of metastasis. Nat. Rev. Cancer *9*, 239–252.

Kerbel, R.S. (2005). Therapeutic implications of intrinsic or induced angiogenic growth factor redundancy in tumors revealed. Cancer Cell *8*, 269–271.

Klysz, D., Tai, X., Robert, P.A., Craveiro, M., Cretenet, G., Oburoglu, L., Mongellaz, C., Floess, S., Fritz, V., Matias, M.I., et al. (2015). Glutamine-dependent α-ketoglutarate production regulates the balance between T helper 1 cell and regulatory T cell generation. Sci. Signal. *8*, ra97.

Kocher, T., Schraml, P., Spagnoli, G.C., Harder, F., and Heberer, M. (2000). Identification of genes differentially expressed in melanoma sublines derived from a single surgical specimen characterised by different sensitivity to cytotoxic T-lymphocyte activity. Schweiz. Med. Wochenschr. *130*, 617–624.

Kreider, T., Anthony, R.M., Urban, J.F., Jr., and Gause, W.C. (2007). Alternatively activated macrophages in helminth infections. Curr. Opin. Immunol. *19*, 448–453.

Kung, H.N., Marks, J.R., and Chi, J.T. (2011). Glutamine synthetase is a genetic determinant of cell type-specific glutamine independence in breast epithelia. PLoS Genet. *7*, e1002229.

Laoui, D., Van Overmeire, E., Di Conza, G., Aldeni, C., Keirsse, J., Morias, Y., Movahedi, K., Houbracken, I., Schouppe, E., Elkrim, Y., et al. (2014). Tumor

hypoxia does not drive differentiation of tumor-associated macrophages but rather fine-tunes the M2-like macrophage population. Cancer Res. *74*, 24–30.

Le, A., Lane, A.N., Hamaker, M., Bose, S., Gouw, A., Barbi, J., Tsukamoto, T., Rojas, C.J., Slusher, B.S., Zhang, H., et al. (2012). Glucose-independent glutamine metabolism via TCA cycling for proliferation and survival in B cells. Cell Metab. *15*, 110–121.

Leite de Oliveira, R., Deschoemaeker, S., Henze, A.-T., Debackere, K., Finisguerra, V., Takeda, Y., Roncal, C., Dettori, D., Tack, E., Jönsson, Y., et al. (2012). Gene-targeting of Phd2 improves tumor response to chemotherapy and prevents side-toxicity. Cancer Cell *22*, 263–277.

Liu, C., Wu, W., Zhang, B., Xiang, J., and Zou, J. (2013). Temporospatial expression and cellular localization of glutamine synthetase following traumatic spinal cord injury in adult rats. Mol. Med. Rep. *7*, 1431–1436.

Locati, M., Mantovani, A., and Sica, A. (2013). Macrophage activation and polarization as an adaptive component of innate immunity. Adv. Immunol. *120*, 163–184.

Martinez, F.O., Gordon, S., Locati, M., and Mantovani, A. (2006). Transcriptional profiling of the human monocyte-to-macrophage differentiation and polarization: new molecules and patterns of gene expression. J. Immunol. *177*, 7303–7311.

Mazzone, M., Dettori, D., de Oliveira, R.L., Loges, S., Schmidt, T., Jonckx, B., Tian, Y.-M., Lanahan, A.A., Pollard, P., de Almodovar, C.R., et al. (2009). Heterozygous deficiency of PHD2 restores tumor oxygenation and inhibits metastasis via endothelial normalization. Cell *136*, 839–851.

McGettrick, A.F., and O'Neill, L.A.J. (2013). How metabolism generates signals during innate immunity and inflammation. J. Biol. Chem. *288*, 22893–22898.

Menga, A., Iacobazzi, V., Infantino, V., Avantaggiati, M.L., and Palmieri, F. (2015). The mitochondrial aspartate/glutamate carrier isoform 1 gene expression is regulated by CREB in neuronal cells. Int. J. Biochem. Cell Biol. *60*, 157–166.

Metzler, B., Gfeller, P., and Guinet, E. (2016). Restricting glutamine or glutamine-dependent purine and pyrimidine syntheses promotes human T cells with high FOXP3 expression and regulatory properties. J. Immunol. *196*, 3618–3630.

Mills, E.L., Kelly, B., Logan, A., Costa, A.S.H., Varma, M., Bryant, C.E., Tourlomousis, P., Däbritz, J.H.M., Gottlieb, E., Latorre, I., et al. (2016). Succinate dehydrogenase supports metabolic repurposing of mitochondria to drive inflammatory macrophages. Cell *167*, 457–470.e13.

Murphy, C., and Newsholme, P. (1998). Importance of glutamine metabolism in murine macrophages and human monocytes to L-arginine biosynthesis and rates of nitrite or urea production. Clin. Sci. *95*, 397–407.

Norenberg, M.D., Jayakumar, A.R., Rama Rao, K.V., and Panickar, K.S. (2007). New concepts in the mechanism of ammonia-induced astrocyte swelling. Metab. Brain Dis. *22*, 219–234.

O'Neill, L.A., and Hardie, D.G. (2013). Metabolism of inflammation limited by AMPK and pseudo-starvation. Nature *493*, 346–355.

O'Neill, L.A.J., and Pearce, E.J. (2016). Immunometabolism governs dendritic cell and macrophage function. J. Exp. Med. *213*, 15–23.

Olney, J.W. (1990). Excitotoxicity: an overview. Can. Dis. Wkly. Rep. *16* (*Suppl 1E*), 47–57, discussion 57–58.

Palmieri, E.M., Spera, I., Menga, A., Infantino, V., Iacobazzi, V., and Castegna, A. (2014). Glutamine synthetase desensitizes differentiated adipocytes to proinflammatory stimuli by raising intracellular glutamine levels. FEBS Lett. *588*, 4807–4814.

Palmieri, E.M., Spera, I., Menga, A., Infantino, V., Porcelli, V., Iacobazzi, V., Pierri, C.L., Hooper, D.C., Palmieri, F., and Castegna, A. (2015). Acetylation of human mitochondrial citrate carrier modulates mitochondrial citrate/malate exchange activity to sustain NADPH production during macrophage activation. Biochim. Biophys. Acta *1847*, 729–738.

Palmieri, E.M., Menga, A., Lebrun, A., Hooper, D.C., Butterfield, D.A., Mazzone, M., and Castegna, A. (2017). Blockade of glutamine synthetase enhances inflammatory response in microglial cells. Antioxid. Redox Signal. *26*, 351–363.

Pollard, J.W. (2004). Tumour-educated macrophages promote tumour progression and metastasis. Nat. Rev. Cancer *4*, 71–78.

Prosniak, M., Harshyne, L.A., Andrews, D.W., Kenyon, L.C., Bedelbaeva, K., Apanasovich, T.V., Heber-Katz, E., Curtis, M.T., Cotzia, P., and Hooper, D.C. (2013). Glioma grade is associated with the accumulation and activity of cells bearing M2 monocyte markers. Clin. Cancer Res. *19*, 3776–3786.

Qian, B.-Z., Zhang, H., Li, J., He, T., Yeo, E.-J., Soong, D.Y.H., Carragher, N.O., Munro, A., Chang, A., Bresnick, A.R., et al. (2015). FLT1 signaling in metastasis-associated macrophages activates an inflammatory signature that promotes breast cancer metastasis. J. Exp. Med. *212*, 1433–1448.

Ries, C.H., Cannarile, M.A., Hoves, S., Benz, J., Wartha, K., Runza, V., Rey-Giraud, F., Pradel, L.P., Feuerhake, F., Klaman, I., et al. (2014). Targeting tumor-associated macrophages with anti-CSF-1R antibody reveals a strategy for cancer therapy. Cancer Cell *25*, 846–859.

Rolny, C., Mazzone, M., Tugues, S., Laoui, D., Johansson, I., Coulon, C., Squadrito, M.L., Segura, I., Li, X., Knevels, E., et al. (2011). HRG inhibits tumor growth and metastasis by inducing macrophage polarization and vessel normalization through downregulation of PlGF. Cancer Cell *19*, 31–44.

Sica, A., and Mantovani, A. (2012). Macrophage plasticity and polarization: in vivo veritas. J. Clin. Invest. *122*, 787–795.

Takeda, N., O'Dea, E.L., Doedens, A., Kim, J.W., Weidemann, A., Stockmann, C., Asagiri, M., Simon, M.C., Hoffmann, A., and Johnson, R.S. (2010). Differential activation and antagonistic function of HIF-alpha isoforms in macrophages are essential for NO homeostasis. Genes Dev. *24*, 491–501.

Takeda, Y., Costa, S., Delamarre, E., Roncal, C., Leite de Oliveira, R., Squadrito, M.L., Finisguerra, V., Deschoemaeker, S., Bruyère, F., Wenes, M., et al. (2011). Macrophage skewing by Phd2 haplodeficiency prevents ischaemia by inducing arteriogenesis. Nature *479*, 122–126.

Tannahill, G.M., Curtis, A.M., Adamik, J., Palsson-McDermott, E.M., McGettrick, A.F., Goel, G., Frezza, C., Bernard, N.J., Kelly, B., Foley, N.H., et al. (2013). Succinate is an inflammatory signal that induces IL-1β through HIF-1α. Nature *496*, 238–242.

van der Vos, K.E., Eliasson, P., Proikas-Cezanne, T., Vervoort, S.J., van Boxtel, R., Putker, M., van Zutphen, I.J., Mauthe, M., Zellmer, S., Pals, C., et al. (2012). Modulation of glutamine metabolism by the PI(3)K-PKB-FOXO network regulates autophagy. Nat. Cell Biol. *14*, 829–837.

Wellen, K.E., and Thompson, C.B. (2012). A two-way street: reciprocal regulation of metabolism and signalling. Nat. Rev. Mol. Cell Biol. *13*, 270–276.

Wenes, M., Shang, M., Di Matteo, M., Goveia, J., Martín-Pérez, R., Serneels, J., Prenen, H., Ghesquière, B., Carmeliet, P., and Mazzone, M. (2016). Macrophage metabolism controls tumor blood vessel morphogenesis and metastasis. Cell Metab. *24*, 701–715.

Wyckoff, J., Wang, W., Lin, E.Y., Wang, Y., Pixley, F., Stanley, E.R., Graf, T., Pollard, J.W., Segall, J., and Condeelis, J. (2004). A paracrine loop between tumor cells and macrophages is required for tumor cell migration in mammary tumors. Cancer Res. *64*, 7022–7029.

Cell Reports, Volume *20*

Supplemental Information

Pharmacologic or Genetic Targeting of Glutamine Synthetase Skews Macrophages toward an M1-like Phenotype and Inhibits Tumor Metastasis

Erika M. Palmieri, Alessio Menga, Rosa Martín-Pérez, Annamaria Quinto, Carla Riera-Domingo, Giacoma De Tullio, Douglas C. Hooper, Wouter H. Lamers, Bart Ghesquière, Daniel W. McVicar, Attilio Guarini, Massimiliano Mazzone, and Alessandra Castegna

SUPPLEMENTAL INFORMATION
Figure S1 related to Fig. 1

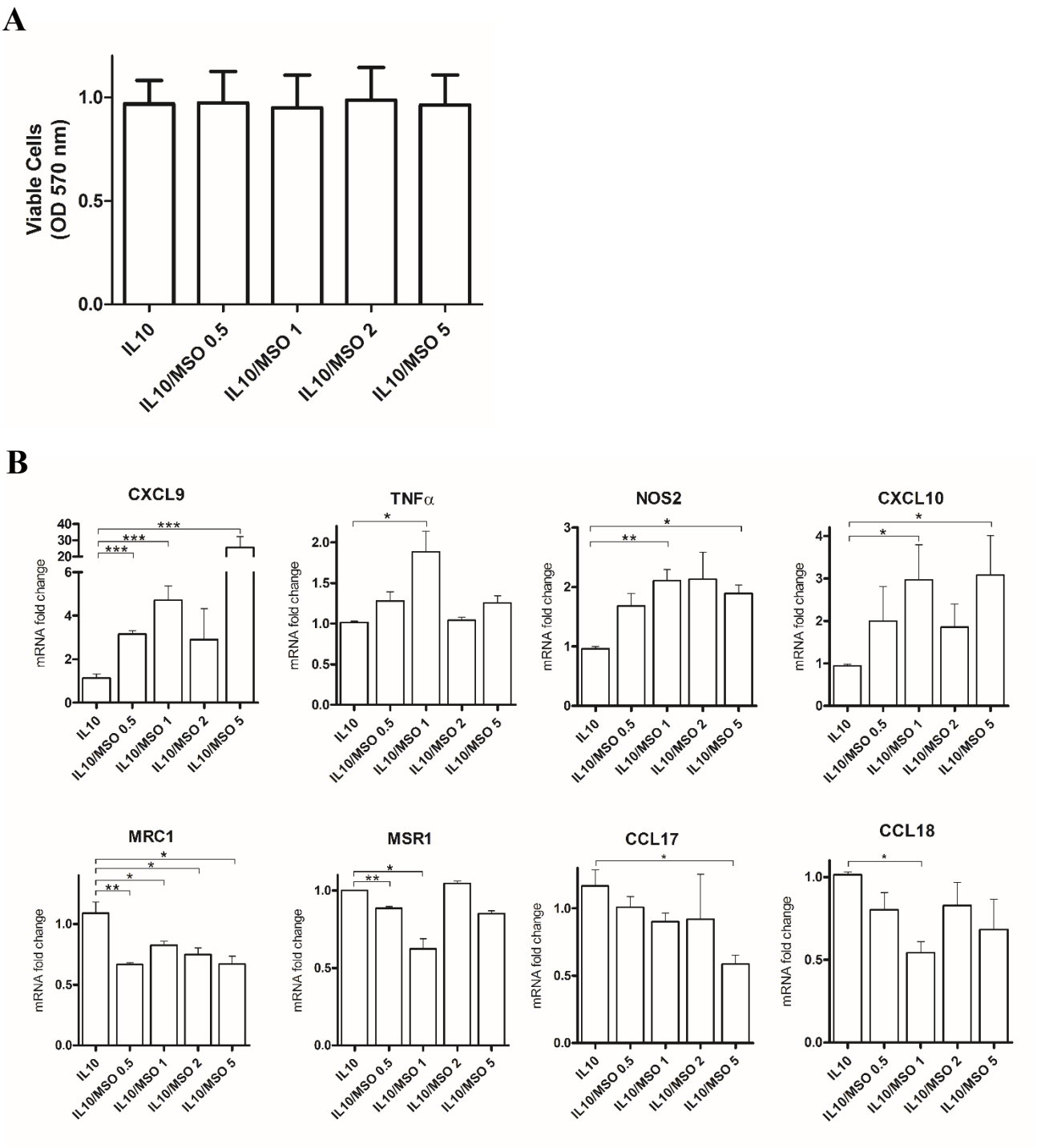

Fig S1 related to Fig. 1
MSO dose response in IL10-treated macrophages
(A) Viability of IL10 macrophages in the presence of MSO at different concentrations.
(B) RT-PCR quantification of M1 or M2 markers in macrophages.
Top, fold increase of M1 markers mRNA in IL10 and MS0-treated IL10 at 4 increasing concentrations of MSO following 24 h of activation (n=3).
Bottom, fold reduction of MSR1, MRC1, CCL17 and CCL18 mRNA in IL10 and MS0-treated IL10 macrophages at 4 increasing concentrations of MSO following 24 h of activation (n=3).

Data are means ± SEM. *p<0.05, **p<0.001, ***p < 0.0001 versus WT.

Figure S2 related to Figure 2

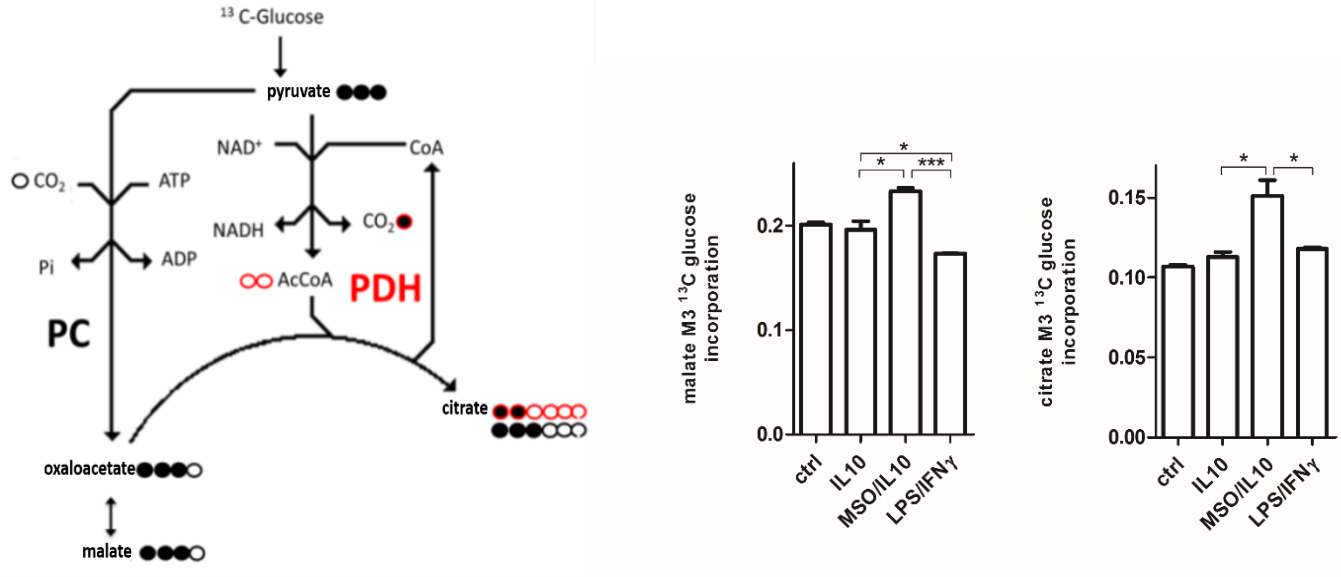

Fig S2 related to Figure 2
GS inhibition reprograms pyruvate metabolism in IL10-treated macrophages

Evaluation of the (M+3) 13C enrichment from [U-13C]-glucose in malate and citrate (n=3).

Data are means ± SEM. *p < 0.05, **p < 0.001, ***p < 0.0001.

Fig S3 related to Figure 6

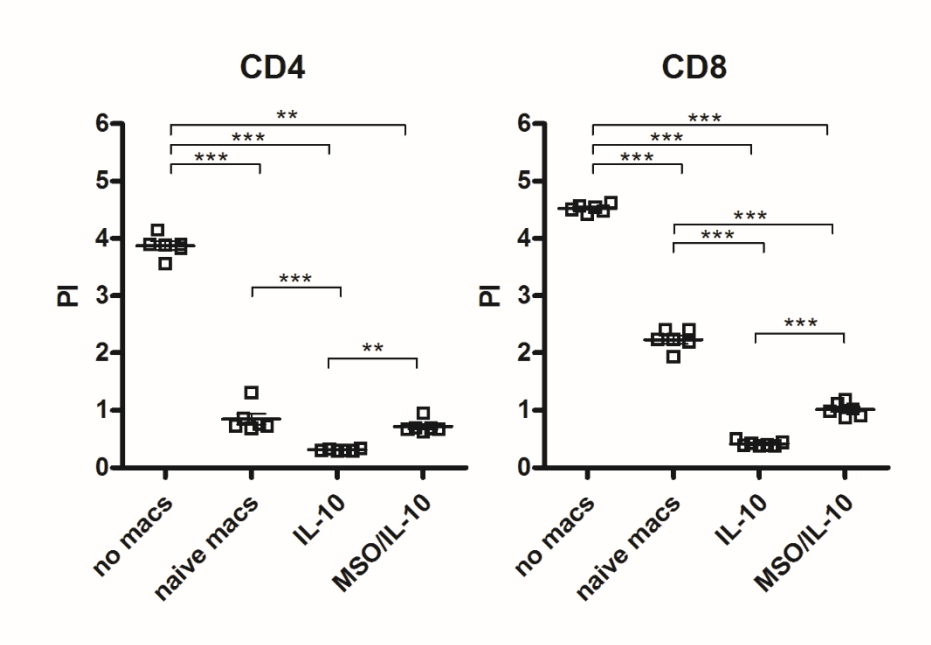

Fig S3 related to Figure 6
Proliferation index of $CD4^+$ and $CD8^+$ cells
Evaluation of the proliferation index (PI) of $CD4^+$ and $CD8^+$ cells co-cultured with IL10 and MSO/IL10 macrophages

Data are means ± SEM. **p < 0.001, ***p < 0.0001 versus no macs

Figure S4 related to Figure 7

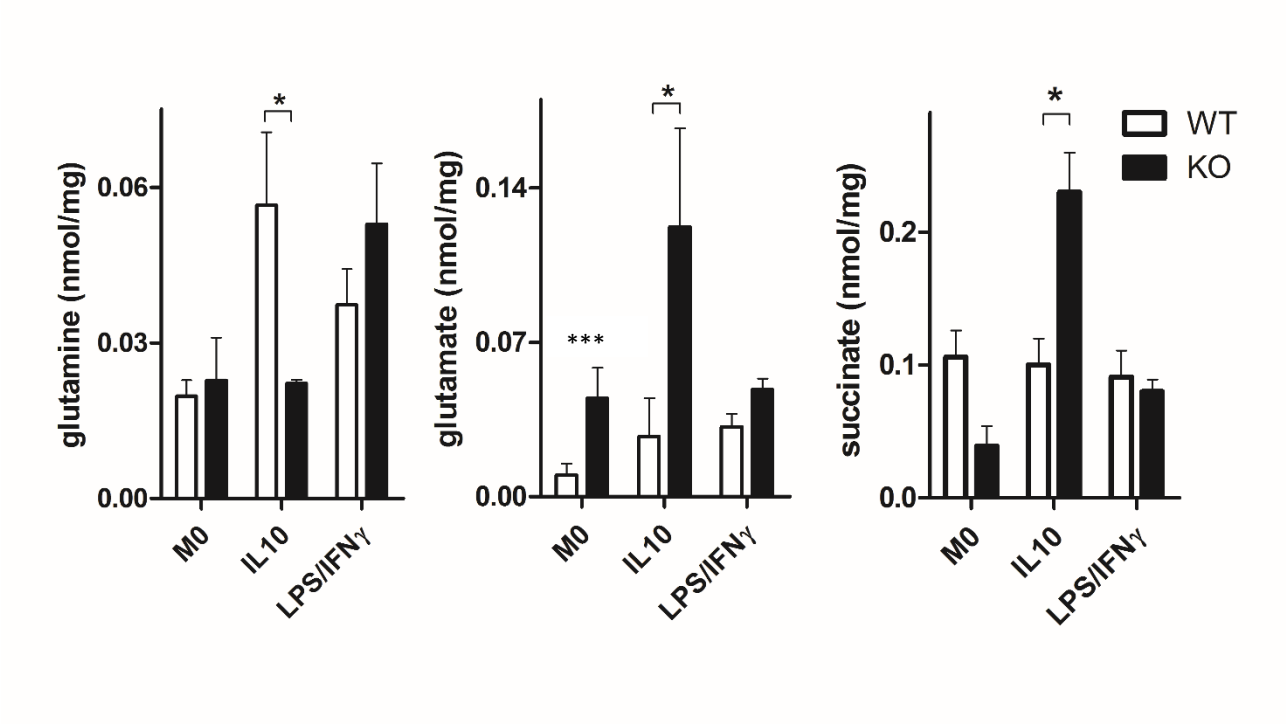

Figure S4, related to Figure 7
Metabolite quantification in WT and cKO BMDMs
Intracellular glutamine, glutamate and succinate levels in BMDMs isolated from WT and cKO mice after 5-day in vivo treatment with tamoxifen (n=3), and treated with IL10 or LPS/IFNγ for 24 h (n=6).

Data are means ± SEM. *p<0.05, ***p < 0.0001 versus WT.

Figure S5 related to Figure7

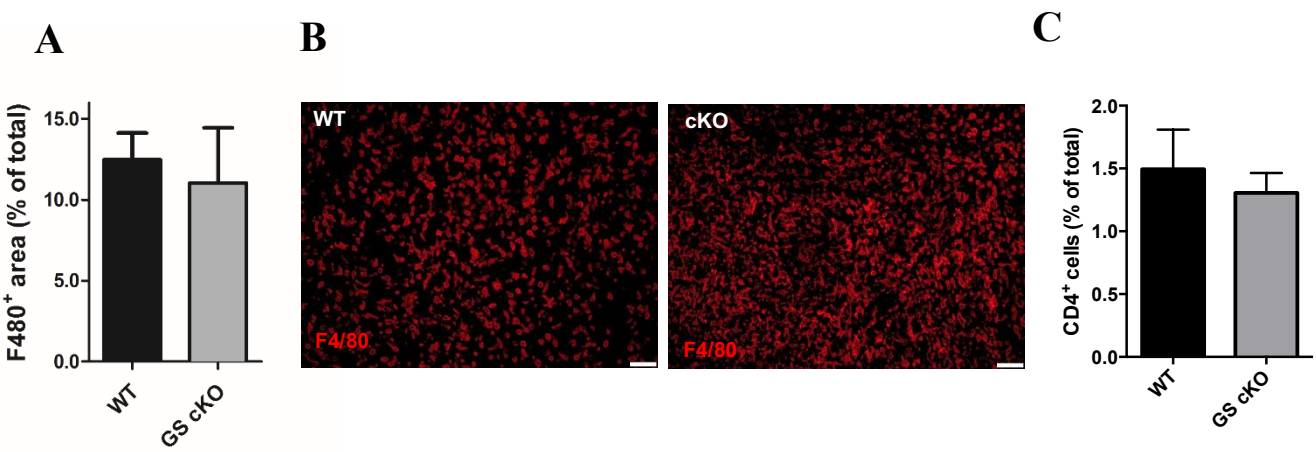

Figure S5, related to Figure 7

F4/80$^+$ tumor areas and CD4+ cells in WT and cKO mice

(A) Quantification and (B) representative images of F4/80$^+$ tumor areas in wild type (HET) and macrophage-specific knock out (cKO) mice (n=8). N represents the number of animals. 6 images per tumor were analyzed. (C) CD4+ cell quantification in wild type (HET) and macrophage-specific knock out (cKO) mice (n=4).

Data are means ± SEM.

Figure S6 related to Fig. 7

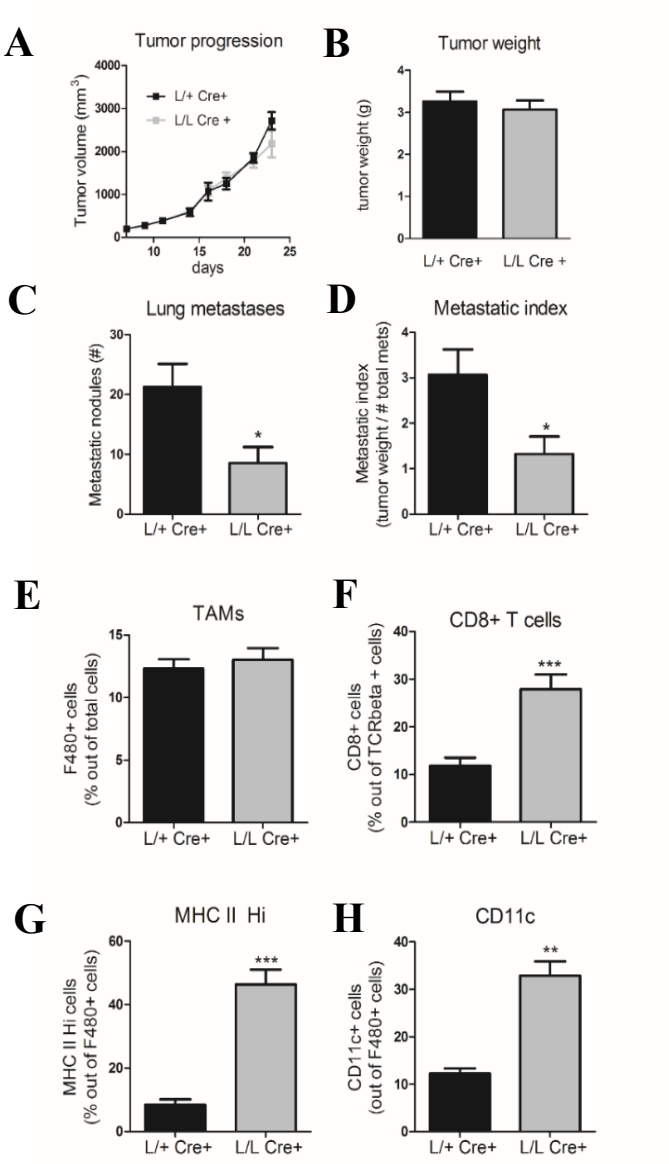

Figure S6. Genetic deletion of GS (L/L Cre+) in TAMs induces the M1-like phenotype, CTL accumulation, and inhibits metastasis.

(A,B) Subcutaneous LLC tumor growth over the time (A) and end-stage tumor weight (B) in L/+ Cre+ (HET) and macrophage-specific knock out (L/L Cre+) mice (n=12). (C,D) Number of lung metastases (C) and lung metastatic index (which is the number of lung metastatic nodules divided for the corresponding tumor weight) (D) in L/+ Cre+ (HET) and macrophage-specific knock out (L/L Cre+) mice (n=12). (E-H) FACS quantification of total F4/80^{+} TAMs (E), CD8^{+} cytotoxic T cells (F), M1-like MHC-II^{high} TAMs (G) and CD11c^{+} TAMs (H) in L/+ Cre+ (HET) and macrophage-specific knock out (L/LCre+) mice (n=6).

Figure S7 related to Fig. 7

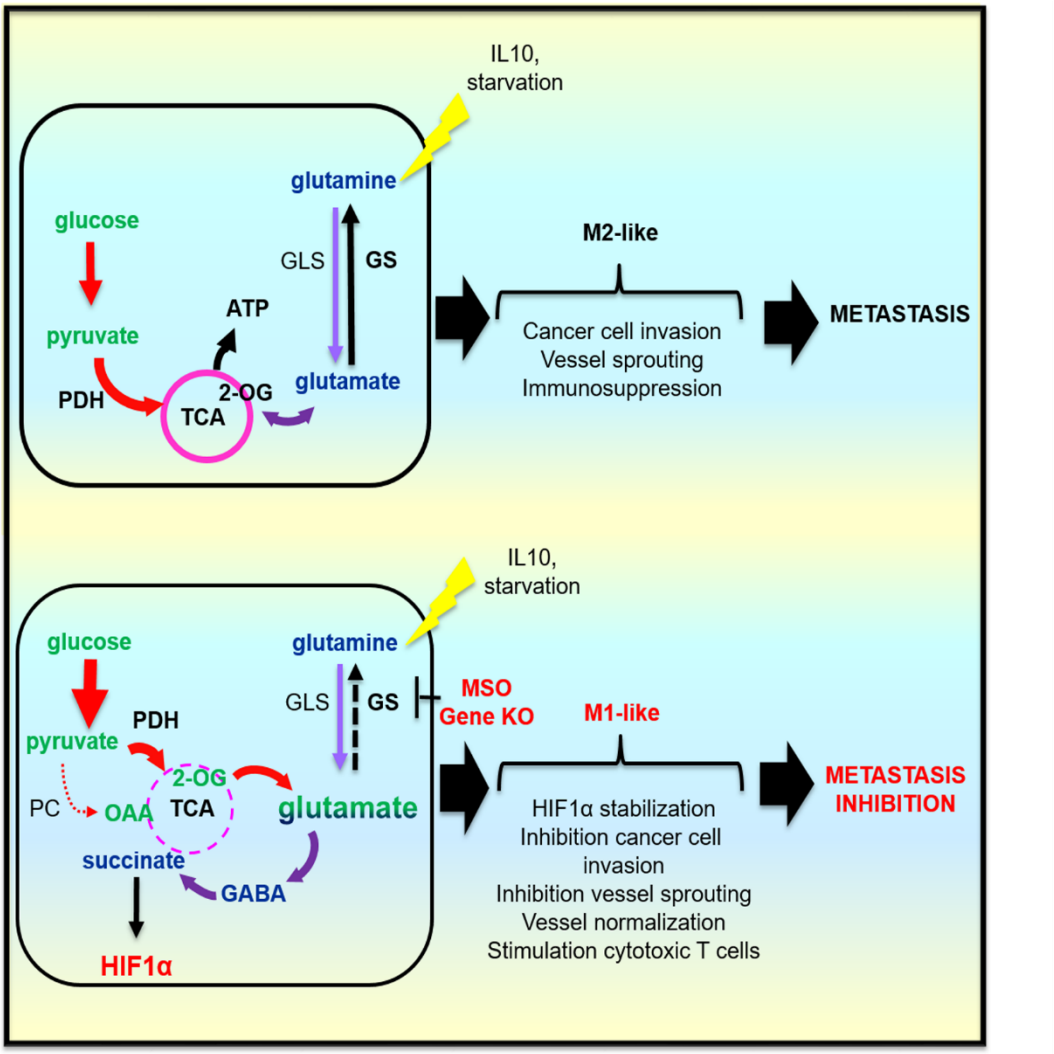

Figure S7. Functional role of metabolic reprogramming following GS inhibition in IL10 macrophages.

(Upper panel) IL10 treatment increases GS expression and activity. Channeling of nutrients toward the TCA cycle for ATP production is favored. Since GS is sensitive to nutrient starvation, decreased nutrient availability by cancer cell might enhance GS expression.

(Lower panel) In vitro GS inhibition lowers intracellular glutamine while increasing glutamate levels. Reduction of glutamine levels increases glucose flux toward glutamate, which strongly accumulates in the cell. Glutamine uptake is not decreased but channeled toward succinate synthesis through GABA. Functionally, GS inhibition or gene deletion reduces M2 and increases M1 markers through stabilization of HIF1α, leading to lower T cell suppression, reduction of angiogenesis with features of tumor vessel normalization, and inhibition of cancer cell invasiveness. Altogether, this translates in a strong inhibition of metastasis formation in mice.

SUPPLEMENTAL EXPERIMENTAL PROCEDURES

Cell preparation

Human blood samples were obtained from healthy individuals under an Institutional Review Board approved protocol and the informed consent was obtained from all subjects involved.
Human monocytes were obtained from healthy blood donor buffy coats by two-step gradient centrifugation using ficoll followed by an additional step using the magnetically isolation with CD14 MicroBeads (Miltenyi Biotec Inc.) as previously described (Palmieri et al., 2015). Finally, monocytes (98% CD14+, 13% CD16+) were seeded in RPMI 10% FBS, 2 mM L-Glutamine with Pen/Strep at a concentration of 4×105 cells/ml for 6 days in the presence of either 1000 U/ml rHuGM-CSF (M1) or 100 ng/ml rHuM-CSF (M2). Then 50% by volume of fresh M1 or M2 medium was added. Macrophage polarization was obtained by culturing cells for an additional 24 h in RPMI 1640 stimulated with 100 ng/mL LPS plus 20 ng/mL IFNγ (for M1 polarization) or either 20 ng/mL IL-4, 20 ng/mL IL-13, 10 ng/mL IL-10 or a combination of both IL-4 and IL-10 (for M2 polarization).
Changes in cell morphology were assessed by phase contrast microscopy (Axiovert 135, Zeiss). Phenotypical and functional characterization of MDM was performed after either 6h, 24h, 48h after activation with cytokines.
For MSO treatment, a stock 200mM MSO solution was prepared in ultrapure water and stored in aliquots at -80°C. ACF was dissolved in water to a stock concentration of 10 mM and stored at -20°C. Dimethylglutamate (DMG) was dissolved in water to a stock concentration of 200 mM and stored at -20°C. Where indicated the cells were stimulated with IL10 with and/or without previous 2h incubation with 5mM DMG.
Cell viability was determined after 72 h of incubation, using the CellTiter 96® Non-Radioactive Cell Proliferation Assay (Promega) as described in (Menga et al., 2017; Palmieri et al., 2017).

Murine bone marrow-derived macrophages (BMDMs) were derived from bone marrow precursors as described before (Meerpohl et al., 1976). Briefly, bone marrow cells (1.6 x106 cells/ml) were cultured in DMEM supplemented with 20% FBS and 30% L929 conditioned medium as a source of M-CSF. After 3 days of culture, an additional 3 ml of differentiation medium was added. At day 7, macrophages were treated with 10 ng/mL IL10 or with 100 ng/mL LPS plus 20 ng/mL IFNγ for 24 h and finally harvested with ice cold Ca^{2+} and Mg^{2+}-free PBS.
Spleens were flushed with 200 U ml−1 collagenase III (Worthington) and left for 30 min at 37 °C. Afterwards, spleens were filtered and red blood cells were removed using erythrocyte lysis buffer.

Flow cytometry

Expression of CD14, CD163, CD80, CD3, CD4, CD8, CD25 on either macrophages or T cell surfaces was studied by flow cytometry. Purified cells following specific treatments were washed with FACS buffer and 3×10^5 cells labeled with fluorescence-labeled anti-human antibody (8 µl) for 30 min at 4°C in dark as per manufacturer's recommendation. After labeling, cells were washed with PBS, resuspended in 300 µL of the same saline solution until acquisition which was performed using a 8 colors flow cytometer (Navios, Beckman Coulter). Data analysis was performed with Kaluza software (Beckman Coulter). Suitable negative iso-type controls were used to rule out the background fluorescence for the used fluorochromes (FITC, PE, PE-Cy5, PE-Cy7 and APC). To ensure that analyses were made only of viable cells and not debris, all events labelled with 7AAD were excluded. Percentage of each positive population and mean fluorescence intensity (MFI) were determined using quadrant statistics.

For surface marker characterization of effector cell subsets, CD4+ and CD8+ T cells were activated with anti-CD3/CD28 Dynabeads (Life Technologies) for 5 days in the presence or absence of macrophages differentiated with different stimuli and stained with the following antibodies: anti-CD25 BV650 (Biolegend), anti-CD69 APC, anti-CD4 PE, and CD8 PE (Becton Dickinson). Cells were analyzed on an LSRII or a Fortessa. Live cells were analyzed by gating on Sytox green negative cells (Life Technologies) and single cells were determined using forward scatter height by area gating strategy. To compensate for possible differences in cell sizes, geometric mean or median fluorescence intensities (MFI) were normalized to forward scatters.

^{13}C tracing experiments

For ^{13}C-carbon incorporation from glucose and glutamine in metabolites, cells were incubated for 48 hours (day 6 of differentiation) with labeled substrates (confirmation of steady state). The exposure to cytokines for macrophage activation was performed in the last 24 hours. For mass spectrometry analysis cells were scraped in 80% methanol and phase separation was achieved by centrifugation at 4°C and the methanol-water phase containing polar metabolites was separated and dried using a vacuum concentrator. For media extraction, 50µL of medium was extracted with methanol

and treated as above. The dried metabolite samples were stored at −80°C. Isotopomer distributions and metabolite levels were measured with a 7890A GC system (Agilent Technologies) combined with a 5975C Inert MS system (Agilent Technologies, Inc.) (Schoors et al., 2015) or with a UPLC system (Acquity, Waters) interfaced with a Quattro Premier mass spectrometer (Waters)
(Palmieri et al., 2015; Palmieri et al., 2014).

T cell purification and expansion

CD4+ naïve autologous T cells were isolated by negative isolation from the PBMC fraction using the CD4+ T Cell Isolation Kit II, human (Miltenyi) according to the manufacturer's instructions. This kit removes cells expressing CD8, CD14, CD16, CD19, CD36, CD56, CD123, TCRγ/δ and CD235a (Glycophorin A). Autologous CD8+ were isolated by negative selection in a similar manner using CD8+ T Cell Isolation Kit, human (Miltenyi). Fresh cells after isolation were then washed with PBS and labeled with 10 µM Cell Trace (CTV: CellTrace™ Violet Cell Proliferation Kit - Life Technologies) as previously described (Quah and Parish, 2012) and resuspended in RPMI 1640 medium supplemented with 10% FCS, 10 mM HEPES, 2 mM glutamine and non-essential amino acids. Labeled cells were used for setup of suppression assays. To address the immunopromoting function of macrophages, cultured primary macrophages either naïve/resting or polarized into M2(IL-10) and M2(IL-10) plus MSO seeded in 96- well plates ($2x10^5$ /ml) were cocultured either with CD4+ or CD8+ T cells in stimulator– responder ratios of 1:2. Macrophage stimulants were washed away extensively (two washings each with addition of 200µl of macrophage media) and complete removal of the medium from the cells was performed before adding T cell suspensions in a final volume of 200µl. Cells were cocultured for 5 days in the presence of anti-CD3/CD28 Dynabeads (Life Technologies)(Volpe et al., 2008) and rhIL-2 25U/ml for activation. As controls, $1x10^5$ $CD4^+$ or $CD8^+$ T cells/well were also plated without macrophages and left alone throughout the entire procedure. T cells were collected after 5 d in culture, washed in MACS buffer, labeled for flow cytometry, and suppression was analyzed for CVT-based proliferation and activation was assessed by staining for CD69. Proliferation index was calculated according to (Burt et al., 2010)

T cell migration assay

Migration of $CD8^+$ cells was assessed by using Transwell Permeable supports with 5-µm Polycarbonate Membrane (Costar). To determine cell migration in response to soluble factors secreted by macrophages, the last were precultured in the lower chamber for 7 days in RPMI 10% FBS and then activated for 8h with LPS/IFNγ or IL10 with or without MSO. Then the medium has been changed and after 18 hours autologous $CD8^+$ cells at 48h hours culture after isolation in the presence of anti CD3 (1µg/mL) and anti CD28 (1µg/mL) were placed in the upper chamber ($2x10^5$ cells in 70 µl of medium with 10% FBS). Macrophages and $CD8^+$ cells were incubated for 3h at 37°C and migrated cells were collected and counted under the microscope (Finisguerra et al., 2015).

Cancer cell invasion assay

The upper side of a Transwell chamber with a 8.0 µm-porous polycarbonate membrane filter (Costar®) was coated with 5 µg Matrigel (Matrix Growth Factor Reduced from Corning®). Different polarization states and MSO pretreated macrophages were detached in cold PBS and then added ($5 X 10^4$/well) together with calcein-labeled A549 cells ($1 x 10^5$/well) to the upper chamber in RPMI medium supplemented with 2% FBS. RPMI medium supplemented with 10% FBS was added to the lower well to create a gradient of serum as chemoattractant stimulus. The migration of A549 cells was assayed after 24 h of incubation. At this time point, the membranes were removed and stained with DAPI, and the number of cells that had invaded the lower chamber was counted in three randomly selected fields under a fluorescence microscopy.

Tumor model

$1x10^6$ Lewis lung carcinoma (LLC) adherent growing murine cells were injected subcutaneously at the right side of the mouse in a volume of 200 µl of PBS. Tumor volumes were measured three times a week with a caliper and calculated using the formula: $V=\pi x(d2 x D)/ 6$, where d is the minor tumor axis and D is the major tumor axis. At the end stage, tumor weight was registered and samples were collected for histological examination. Lung metastasis nodules were contrasted after intratracheal injection of 15% India ink solution. Superficial metastatic nodules were assessed under a stereomicroscope.

FACS analysis and flow sorting of tissue- and tumor-associated macrophages

LLC tumor-bearing mice were sacrificed by cervical dislocation and tumors were harvested. Tumors or other organs were minced in RPMI medium containing 0.1% collagenase type I and 0,2% dispase type I and incubated in the same solution for 30 minutes at 37°C. Samples from spleen were mechanically dissociated. The digested or dissociated tissue was filtered using a 70 µm pore sized mesh and cells were centrifuged 5 min at 1000 rpm. Red blood cell lysis was performed by using Hybri-Max^{TM} (Sigma-Aldrich). For flow sorting, the myeloid cell population in the tumor single cell suspension, and when appropriate in flushed splenocytes, was enriched by coating with CD11b-conjugated magnetic beads (MACS, Miltenyi Biotec) and separation through magnetic columns (MACS, Miltenyi Biotec). Cells were resuspended in FACS buffer (PBS containing 2% FBS and 2 mM EDTA) and incubated for 15 minutes with Mouse BD Fc Block™ purified anti-mouse CD16/CD32 mAb (BD-pharmingen) and stained with the following antibodies for 20 minutes at 4 °C: anti-F4/80, anti-CD3, anti-CD4, anti-CD8, anti-MHCII, anti-CD206, anti-CD11c (all eBioscience), and anti-CD31 (BD-pharmingen). Cells were subsequently washed and resuspended in cold FACS buffer before FACS analysis or flow sorting by a FACS Verse or FACS Aria (BD Biosciences), respectively.

Histology and immunostainings

For serial sections cut at 7 µm thickness, tissue samples were fixed in 2% PFA overnight at 4°C, dehydrated and embedded in paraffin. Paraffin slides were first rehydrated to further proceed with antigen retrieval in citrate solution (DAKO). The sections were blocked with the appropriate serum (DAKO) and incubated overnight with the following antibodies: rat anti-CD31 (BD Pharmingen) 1:200, rabbit anti-FITC (Serotec) 1:200, rat anti-F4/80 (Serotec) 1:100, rabbit anti-hypoxyprobe (HPI) 1:100, goat anti-CD105 (R&D Systems) and rat anti-TER119 (R&D Systems). Appropriate secondary antibodies were used: Alexa 488, 647 or 568 conjugated secondary antibodies (Molecular Probes) 1:200, biotin-labeled antibodies (Jackson Immunoresearch) 1:300 and, when necessary, TCA fluoricine or TSA Plus Cyanine 3 System amplification (Perkin Elmer, Life Sciences) were performed according to the manufacturer's instructions. Whenever sections were stained in fluorescence, ProLong Gold mounting medium with or without DAPI (Invitrogen) was used. Microscopic analysis was done with an Olympus BX41 microscope and CellSense imaging software.

Hypoxia assessment

Tumor hypoxia was detected 1h after i.p. injection of 60 mg/kg pimonidazole hydrochloride into tumor-bearing mice. Mice were sacrificed and tumors harvested. To detect the formation of pimonidazole adducts, tumor paraffin sections were immunostained with Hypoxyprobe-1-Mab1 (Hypoxyprobe kit, Chemicon) following the manufacturer's instructions.

Additional References

Burt, T.D., Seu, L., Mold, J.E., Kappas, A., McCune, J.M., 2010. Naive Human T Cells Are Activated and Proliferate in Response to the Heme Oxygenase-1 Inhibitor Tin Mesoporphyrin. The Journal of Immunology 185, 5279–5288.

Finisguerra, V., Di Conza, G., Di Matteo, M., Serneels, J., Costa, S., Thompson, A.A.R., Wauters, E., Walmsley, S., Prenen, H., Granot, Z., Casazza, A., Mazzone, M., 2015. MET is required for the recruitment of anti-tumoural neutrophils. Nature 522, 349–53.

Meerpohl, H.-G., Lohmann-Matthes, M.-L., Fischer, H., 1976. Studies on the activation of mouse bone marrow-derived macrophages by the macrophage cytotoxicity factor (MCF). European Journal of Immunology 6, 213–217.

Menga, A., Palmieri, E.M., Cianciulli, A., Infantino, V., Mazzone, M., Scilimati, A., Palmieri, F., Castegna, A., Iacobazzi, V., 2017. *SLC25A26* overexpression impairs cell function via mtDNA hypermethylation and rewiring of methyl metabolism. The FEBS Journal.

Quah, B.J.C., Parish, C.R., 2012. New and improved methods for measuring lymphocyte proliferation in vitro and in vivo using CFSE-like fluorescent dyes. Journal of Immunological Methods 379, 1–14.

Volpe, E., Servant, N., Zollinger, R., Bogiatzi, S.I., Hupé, P., Barillot, E., Soumelis, V., 2008. A critical function for transforming growth factor-β, interleukin 23 and proinflammatory cytokines in driving and modulating human TH-17 responses. Nature Immunology 9, 650–657.